UNIVERSITY OF OKLAHOMA GRADUATE COLLEGE

MATERIAL CHARACTERIZATION OF 3D-PRINTED SPECIMENS BASED ON PRINTING ORIENTATION

A THESIS

SUBMITTED TO THE GRADUATE FACULTY

in partial fulfillment of the requirements for the

Degree of

MASTER OF SCIENCE

By Wyatt J Main

Norman, Oklahoma

2025

Downloaded from SHAREOK. Persistent Handle URL: https://hdl.handle.net/11244/341476

MATERIAL CHARACTERIZATION OF 3D-PRINTED SPECIMENS BASED ON PRINTING ORIENTATION

A THESIS APPROVED FOR THE SCHOOL OF AEROSPACE AND MECHANICAL ENGINEERING

BY THE COMMITTEE CONSISTING OF

Dr. J. David Baldwin, Chair

Dr. Ramkumar Parthasarathy

Dr. Mrinal Saha

©Copyright by Wyatt J Main 2025

All Rights Reserved.

Acknowledgements

I would like to thank Dr. J. David Baldwin for serving as my advisor and the head of my committee, as well as his constant and unending support throughout this process. He has made himself and his time available to me so often throughout this process. He was forthcoming with advice on many different topics and was ready to reach out to others whenever we got to anything he was unsure of. I also appreciate his efforts to promote me and suggest methods of advancing my academic and professional development.

I would like to express my appreciation to Dr. Ramkumar Parthasarathy for being willing to serve on my thesis committee. I would also like to thank him for his continuous support of me through my academic life here at the university.

I would also like to thank Dr. Mrinal Saha for serving on my committee so willingly. I also want to thank him for lending me access to his lab and instruments, without which many parts of this research would not have happened. I also want to thank him for putting me in touch with Anirban Mondal.

I would like to thank Anirban Mondal who made himself available to me and mentored me on the molding, polishing, and microscopy processes used in this research. Without him those steps might not have been possible in the timeframe I had available, as he put in the effort to make sure I understood the processes in a condensed timeframe.

I would like to thank Dr. Liu for his assistance throughout my time at OU, providing access to his labs and 3D-printers, as well as introducing me to Peter Vu.

I would like to thank Peter Vu as he helped me get familiar with the Bambu 3D-printer and the software needed to run it.

I would also like to thank Christian Dix as he helped with the development of the Stress-Strain curves.

I would like to thank my friends and family who have supported me throughout this program and in my general life despite the rough patches.

I would like to thank my parents especially as they have continuously supported me in so many of the things I have done in life and have always had my back.

Finally, I would like to thank the University of Oklahoma for providing me with this opportunity.

Table of Contents

Page #

Acknowledgements iv
List of Figures vii
List of Tables viii
Abstract ix
Chapter 1: Introduction and Background information 1
1.1 Introduction 1
1.2 Background 3
1.3 Research Plan 4
1.3.1 Specimen Fabrication 5
1.3.2 Tensile Testing 5
1.3.3 Specimen Preparation for Microscopy 5
1.3.4 Microscopy 6
Chapter 2: Specimen Fabrication 7
2.1 Specimen Prep 7
2.2 Results 10
Chapter 3: Tensile Testing 13
3.1 Experimental Process and Equipment 13
3.2 Data Analysis 18
3.3 Discussion of Results 23
Chapter 4: Specimen Prep for Microscopy 32
4.1 Molding 32
4.2 Results 39
Chapter 5: Microscopy 41
5.1 Imaging Procedure 41
5.2 Discussion of Results 41
Chapter 6. Concluding remarks 45
6.1 Interpretations 45
6.2 Plans for the future 47
Appendix 50

Appendix 1: Creating an Instron Test Method 50
Appendix 2: Force-Displacement and Strain-Displacement Results 53
Appendix 3: Stress-Strain Curves 63
Appendix 4: Estimates of Young's Modulus 72

List of Figures

Figure 1: Dogbone Specimen Dimensions (mm and degrees) 7
Figure 2: Gage-length Specimen Dimensions (mm and degrees) 8
Figure 3: 3D-Printer in use 9
Figure 4: Freshly Printed Series of Specimens 12
Figure 5: A mounted specimen 16
Figure 6: Extensometer attached to a mounted specimen 17
Figure 7:Force and Strain vs. Displacement plot for the A-0 Specimen 19
Figure 8: Stress - Strain Response of the A-0 Specimen 20
Figure 9: Initial portion of the stress vs. strain plot for A-0 21
Figure 10: Visual representation of tensile strength and strain at fracture 23
Figure 11: Tensile Series A Stress-Strain Comparison 24
Figure 12: Tensile Series B Stress-Strain Comparison 24
Figure 13: Tensile Series C Stress-Strain Comparison 25
Figure 14: Tensile Series D Stress-Strain Comparison 25
Figure 15: Tensile Series E Stress-Strain Comparison 26
Figure 16: Tensile Series F Stress-Strain Comparison 26
Figure 17: 0-Degree Specimens of Each Tensile Series 28
Figure 18: 45- Degree Specimens of Each Tensile Series 29
Figure 19: 90- Degree Specimens of Each Tensile Series 29
Figure 20: A collection of the tensile data for every specimen 30
Figure 21: Orientation of specimens in mold 34
Figure 22: Struers Polisher 35
Figure 23: The Six Molds in the Order A, B, C, D, E, and F 40
Figure 24: Specimen C-0 at 200x magnification 42
Figure 25: Specimen B-45 at 200x magnification 43
Figure 26: Specimen D-90 at 200x magnification 43
Figure 27: Force & Strain vs. Displacement for A-45 53
Figure 28: Force & Strain vs. Displacement for A-90 53
Figure 29: Force & Strain vs. Displacement for B-0 54
Figure 30: Force & Strain vs. Displacement for B-45 54
Figure 31: Force & Strain vs. Displacement for B-90 55
Figure 32: Force & Strain vs. Displacement for C-0 55
Figure 33: Force & Strain vs. Displacement for C-45 56
Figure 34: Force & Strain vs. Displacement for C-90 57
Figure 35: Force & Strain vs. Displacement for D-0 58
Figure 36: Force & Strain vs. Displacement for D-45 58
Figure 37: Force & Strain vs. Displacement for D-90 59
Figure 38: Force & Strain vs. Displacement for E-0 59
Figure 39: Force & Strain vs. Displacement for E-45 60
Figure 40: Force & Strain vs. Displacement for E-90 60
Figure 41: Force & Strain vs. Displacement for F-0 61

Figure 42: Force & Strain vs. Displacement for F-45 61
Figure 43: Force & Strain vs. Displacement for F-90 62
Figure 44: Stress vs. Strain for A-45 63
Figure 45: Stress vs. Strain for A-90 63
Figure 46: Stress vs. Strain for B-0 64
Figure 47: Stress vs. Strain for B-45 64
Figure 48: Stress vs. Strain for B-90 65
Figure 49: Stress vs. Strain for C-0 65
Figure 50: Stress vs. Strain for C-45 66
Figure 51: Stress vs. Strain for C-90 66
Figure 52: Stress vs. Strain for D-0 67
Figure 53: Stress vs. Strain for D-45 67
Figure 54: Stress vs. Strain for D-90 68
Figure 55: Stress vs. Strain for E-0 68
Figure 56: Stress vs. Strain for E-45 69
Figure 57: Stress vs. Strain for E-90 69
Figure 58: Stress vs. Strain for F-0 70
Figure 59: Stress vs. Strain for F-45 70
Figure 60: Stress vs. Strain for F-90 71
Figure 61: Initial portion of the stress vs. strain plot for A-45 72
Figure 62: Initial portion of the stress vs. strain plot for A-90 72
Figure 63: Initial portion of the stress vs. strain plot for B-0 73
Figure 64: Initial portion of the stress vs. strain plot for B-45 73
Figure 65: Initial portion of the stress vs. strain plot for B-90 74
Figure 66: Initial portion of the stress vs. strain plot for C-0 74
Figure 67: Initial portion of the stress vs. strain plot for C-45 75
Figure 68: Initial portion of the stress vs. strain plot for C-90 75
Figure 69: Initial portion of the stress vs. strain plot for D-0 76
Figure 70: Initial portion of the stress vs. strain plot for D-45 76
Figure 71: Initial portion of the stress vs. strain plot for D-90 77
Figure 72: Initial portion of the stress vs. strain plot for E-0 77
Figure 73: Initial portion of the stress vs. strain plot for E-45 78
Figure 74: Initial portion of the stress vs. strain plot for E-90 78
Figure 75: Initial portion of the stress vs. strain plot for F-0 79
Figure 76: Initial portion of the stress vs. strain plot for F-45 79
Figure 77: Initial portion of the stress vs. strain plot for F-90 80

List of Tables

Table 1: Specimen Dimensions 11
Table 2: Material Characteristics derived from the tensile data of the specimens 22

Abstract

A PA12 nylon material blended and reinforced with chopped carbon fibers was prepared as tensile test specimens. Experimentation was performed to investigate what effects the angle (0°, 45°, or 90°) that the material is laid down in when printing has on the mechanical properties of the printed specimens. It was determined that of the three angles investigated, a 0-degree lay down angle to the longitudinal axis results in the stiffest mechanical properties, but can withstand the least strain at fracture. The 90-degree pattern results in the least stiff results, and can withstand more strain than the 0-degree specimen. The 45-degree specimen showed intermediate stiffness and the largest strain at fracture. Microscopy performed on the specimens revealed that the chopped fibers appeared to be randomly organized throughout the specimens.

Chapter 1: Introduction and Background information

1.1 Introduction

Manufacturing is a cornerstone of our modern society. For the vast majority of nonbiological products there is a manufacturing process, and this is especially true in regards to metal products. A lump of raw metal is not what most people want, they want the worked, shaped, and finished products. From a sheet of metal to the bearings of a vehicle's wheels, manufactured products are everywhere. For all of these products there is a process that must be followed to take them from the base materials to a finished product, and for most products of current times this process is subtractive. Subtractive manufacturing means that when someone wants to manufacture a part, they start with a large portion of the material a part is to be made out of, and then shape, cut, and work the material into the final form, removing portions of the material throughout the process. However, while subtractive manufacturing has been the dominant manufacturing process until now, due to being essentially the only method, a new process is arising as additive manufacturing is estimated to show considerable market growth with a compound annual growth rate of 23.3% between 2023 and 2030 [1]. Additive manufacturing works as the reverse of subtractive manufacturing in that it works by taking smaller portions of materials and shaping them into the desired final form while merging them to each other throughout the process. Advantages of additive manufacturing include, but are not limited to, ease of production as products can often be fabricated by a single hands-off machine, lack of required training as complete, simple products can be fabricated using this process with little to no training, and ease of access as additive manufacturing has been growing and is

becoming progressively accessible to the general public. However, additive manufacturing is not solely advantageous, there are also a number of challenges including, but not limited to, a lack of resolution as the process is not yet well suited to detail work, and a high starting cost as while the market for the process is growing, the cost for a personal machine can still be considered more expensive than many can use on a luxury. Probably the most well-known example of additive manufacturing is 3D-printing which has been around since as early as the 1980's [2]. Specifically, polymer 3D-printing is what most people think of when they think of 3D-printing.

Polymer 3D-printing is the process of melting and extruding a melted polymer material onto a bed in a predetermined pattern layer by layer to build a desired product. It is this predetermined pattern part that this research will be focusing on. In this research, the primary question being investigated is whether the angle that the material is laid down in, or raster angle, has any considerable effect on the material characteristics of the final product. The specific angles investigated in this research were 0°, 45°, and 90°. The reason for investigating this is a matter of efficiency and safety. From the standpoint of efficiency, this information should allow a producer to fabricate parts that meet safety requirements while reducing the amount of material used. While from the standpoint of safety, this information should allow a producer to fabricate parts that can better withstand stresses and strains while using the same amount of material. In either case, the information that one can improve their final product in one way or the other by a small change can lead to useful effects.

As this research is focusing on whether or not there are any noticeable effects on the material characteristics based on raster angle two null hypotheses were produced, one

connected to the tensile data and its results and the other connected to the microscopy results. The first null hypothesis of this research is that there is no noticeable effect on the tensile characteristics of the final products based on raster angle. This would be supported by the Tensile results being indistinguishable between different raster angle specimens. The second null hypothesis states that the raster angle has no noticeable effect on the orientation of fibers in the internal structure of the final products. This would be supported if the orientation of the internal fibers was quasi-random and indistinguishable between different raster angles. However, as these are the null hypotheses, testing was required to determine if the results support rejecting these hypotheses, or failing to reject the hypotheses.

1.2 Background

As was previously mentioned, the field of 3D-printing has been growing, and with this growth there has been research into various aspects of the process. These range from investigating the effects of infill patterns [3,4], the effects of fiber reinforcement [5-8], the effects of the distance between the nozzle and bed of the printer [9], to the consistency of material characteristics for printed specimens [10]. Each of these are just a drop in the bucket of the research in this field that continues to grow, but they are evidence of the field continuing to build upon itself.

As is required for the field to grow upon itself, there has been plenty of research into the field, and as such it is not odd for similar research to exist. A particular article of research was done that also looked into the effects of raster angle by Ning et al. [11]. However, in this paper the angles that the authors used were alternating by 90 degrees between each layer. An example of this set up would be that if the bottom layer's raster angle was 0° the next layer would be at 90°. From this alternating raster angle, the authors

had two specimens based on raster angle. These specimens were a [0,90] specimen type and a [-45,45] specimen. The [0,90] specimens had an initial layer with a raster angle of 0° with the following layer having a 90° raster angle. The subsequent layers alternated respectively between these two angles. The [-45,45] specimens followed the same format, but had -45° replacing 0° and 45° replacing 90°. Using this alternating raster angle setup, the authors found that their results showed the [0,90] specimens had greater tensile strength and Young's modulus as well as other data points. On the other hand, they found the [-45,45] specimens had greater toughness and ductility. In comparison, this research will not be alternating the raster angle between layers. For each specimen investigated in this research, the raster angle was the same throughout the whole specimen. Similarly, while Ning, et al. used a 5 wt% chopped carbon fiber reinforced ABS thermoplastic material, this research uses a 20 wt% chopped carbon fiber reinforced nylon material.

1.3 Research Plan

For this research, there were multiple sections to reach the final conclusions. These sections include specimen fabrication, tensile testing, specimen prep for microscopy, and microscopy. Each of these sections contain multiple steps within themselves, and each is interdependent with at least one of the other sections. An example would be that specimen fabrication is connected to tensile testing and specimen prep for microscopy as it is in this section that the specimens that are acted on in those sections are fabricated. However, the internal steps in the sections are primarily disconnected from the other sections. As such, the steps will be described individually in the following sections 1.3.1-1.3.4.

1.3.1 Specimen Fabrication

In this section of the research, the specimens that were used throughout the rest of the research were fabricated. To do this, the specimens were designed as parts in the SOLIDWORKS software, sliced in the OrcaSlicer software, and Printed using a Bambu 3D-printer. Dogbone specimens were designed according to ASTM D638-22 standard along with gage lengths that were meant to represent a non-fractured version of the central bars of the dogbones for the microscopy section. Both were printed at the same time to keep the gage lengths as similar to their respective dogbones as possible.

1.3.2 Tensile Testing

In this section of the research, the fabricated specimens were subjected to tensile testing using an Instron instrument according to a Method that was produced specifically for this research. Tensile testing was performed on each specimen until fracture was achieved. The results of this tensile testing were analyzed using Window's Excel software to determine important material characteristics, e.g. Young's modulus and tensile strength, and plot the tensile testing data for comparison between specimens. It was from these comparison plots that the bulk of conclusions were drawn in this research.

1.3.3 Specimen Preparation for Microscopy

In this section, the gage lengths that were fabricated with their corresponding dogbones were bisected, molded, and polished. The bisected gage lengths were molded using Allied Quickcure before being polished with a Struers polishing instrument to a state that could have microscopy performed on it for clear observation of the internals of the gage lengths. The polishing consisted of using a variety of sandpaper sheets and polishing suspensions ranging from 800 grit sandpaper to 1 micrometer polishing suspension.

1.3.4 Microscopy

In this section of the research, the goal was to observe the state of the carbon fibers in the specimens to determine if the orientation of the carbon fibers was mostly random or if the fibers followed a noticeable pattern dependent on the raster angle of the specimen. This was done in cooperation with the Samuel Roberts Noble Microscopy Lab located on the University of Oklahoma campus. The Keyence microscope available to students at the lab was used to obtain several images at varying magnifications of the gage lengths.

Chapter 2: Specimen Fabrication

This chapter is focused on describing how the specimens were designed, fabricated, and how close the printed specimens were to the desired dimensions. The first section of the chapter describes how the specimens were designed, what they were made of, and how they were fabricated. The second section describes the dimensions of the printed specimens.

2.1 Specimen Prep

For this research, the specimens were initially designed in SOLIDWORKS, and took the form of dogbone testing specimens, as can be seen in the SOLIDWORKS drawing in Figure 1 below. The dogbone specimens had their dimensions dictated by the specifications of the type-1 specimen from ASTM D638-22.

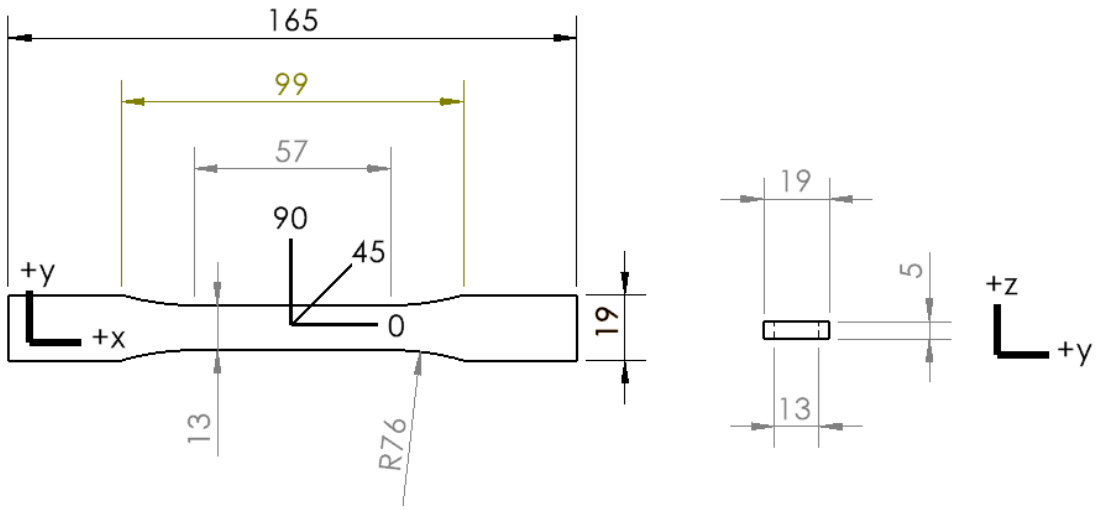

Figure 1: Dogbone Specimen Dimensions (mm and degrees)

Along with the dogbone specimens, gage length specimens were also prepared. These gage length specimens take the form of the central bar of the dogbone specimens and measure as 13x5x50 mm rectangular blocks as can be seen in Figure 2 below.

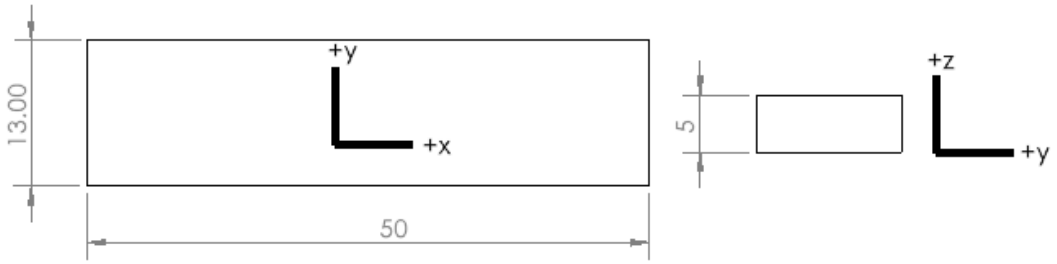

Figure 2: Gage-length Specimen Dimensions (mm and degrees)

These gage lengths were produced to be able to perform microscopy on the interior of the specimens. This was required because performing the interior of the dogbones post tensile testing would be irrevocably affected by any changes that occurred during the tensile testing and subsequent fracture, likely skewing microscopy results. As such, an additional specimen was printed at the same time for each of the dogbone specimens. However, due to the size required for the molding process, and to save material, the ends of the dogbones were removed, leading to the design in Figure 2.

The specimens of this research were made with a chopped carbon fiber reinforced nylon material, specifically the NylonX Carbon Fiber PA12 Filament – 1.75mm (0.5kg) material from matterhackers.com. This material is reported to have a nominal diameter of 1.75mm ± 0.02mm, density of 1.00g/cm^3, melting point of 180°C, Young's (tensile) modulus of 6,000 MPa, and Ultimate (tensile) strength of 100 MPa.

The specimens were printed with a Bambu X-1 Carbon 3D-printer pictured in Figure 3 below.



Figure 3: 3D-Printer in use

Initial prints with this Bambu printer showed that consistency to the desired dimensions was acceptable by being within 1 millimeter in regards to width and thickness and 5 millimeters in regards to overall length of the ASTM standard's dimensions. The width and thickness were measured with a caliper. However, due to the overall length of the specimens no available calipers were able to be used to measure the length. Due to this, a ruler was used instead, despite the level of inaccuracy inherent to it. With the printed specimens being produced within an acceptable level of error, the printing of specimens proceeded.

The dogbones were built to the specifications of the standard in SOLIDWORKS software that can be seen in Figures 1 and 2 above. Once the specimens were built in a SOLIDWORKS file it was uploaded to the printer using the Orcaslicer v2.1.1 software.

Using Orcaslicer, specifications of how each print was to be performed were designated. This functionality was what allowed the raster angle, or the angle that the material was laid down at in reference to the specimen's x-axis, to be specified. The angles that were investigated in this research include 0°, 45°, and 90° from the specimen's x-axis. These angles were applied throughout the infill of the specimens. As an example, for a 0° specimen every layer's material was laid down line by line at 0° to the x-axis. Other than the angles, there were a number of other specifications designated in Orcaslicer for the prints such as having a 5mm wide trimmable brim for more consistent print success, 0.2 mm layer height which produced 25 layers, 0.42mm line width, one top shell layer, 100% infill density, no infill rotation, and only two wall layers. Based off of these specifications, six series of specimens were printed. These specimen series were designated as series A-F.

2.2 Results

This section is dedicated to going over the results of the printing of the six series of specimens, A-F. Located below is Table 1 which lists the width and thickness of the central bar in millimeters of each dogbone that was measured with a caliper, as well as the overall length of the dogbone specimens in centimeters including the wider end sections as well as the central bar. After that is a freshly printed series in Figure 4 to illustrate the state the specimens were in directly out of the printer.

Table 1: Tensile Test Specimen Dimensions

Specimen Series	Angle (degrees)	Width (mm)	Thickness (mm)	Overall Length (cm)
A	0	13.74	5.36	16.5
	45	13.61	5.48	16.5
	90	13.61	5.53	16.5
B	0	13.63	5.51	16.5
	45	13.61	5.55	16.3
	90	13.66	5.54	16.3
C	0	13.65	5.25	16.3
	45	13.54	5.46	16.4
	90	13.61	5.25	16.4
D	0	13.79	5.22	16.5
	45	13.60	5.42	16.4
	90	13.62	5.44	16.4
E	0	13.27	5.02	16.5
	45	13.21	5.33	16.4
	90	13.33	5.29	16.3
F	0	13.50	5.15	16.5
	45	13.21	5.31	16.4
	90	13.36	5.28	16.3

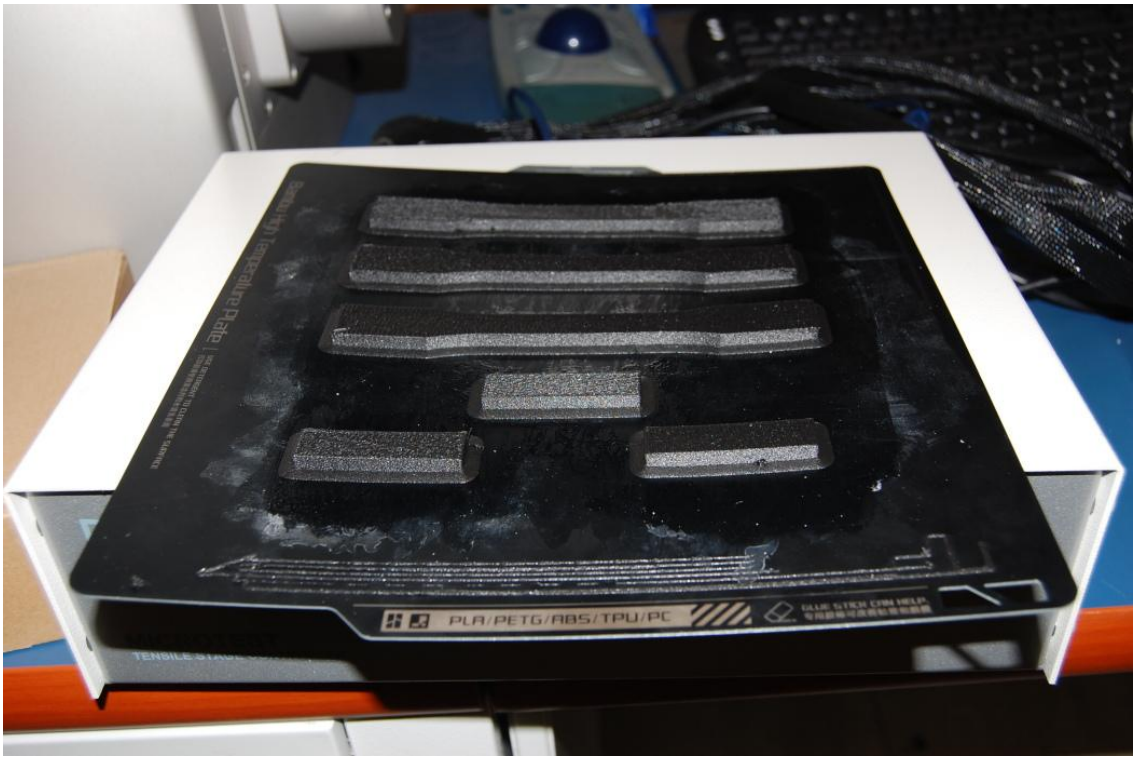

Figure 4: Freshly Printed Series of Specimens

Looking through Table 1 it can be seen that each specimen is within one millimeter for width and thickness and five millimeters for overall length in comparison to the designated standard dimensions. This was deemed acceptable for this research as the material characterization can be done as long as there are accurately measured dimensions for the width and thickness.

Chapter 3: Tensile Testing

This chapter describes the tensile testing that was performed on the specimens, the data that were obtained from the tensile testing, and discusses what the data means for this research.

3.1 Experimental Process and Equipment

With the production of acceptable specimens completed, the next step was obtaining the tensile testing data that forms the backbone of this research. The data were obtained with an Instron 34TM-50. The Instron was equipped with a 50 KN load cell, wedge grips, and was run with Bluehill Universal v4.44 software. The tensile data obtained were specifically force in Newtons, displacement in millimeters, and axial strain in percent. The strain was obtained using an Instron 2630-102 Strain Gauge Extensometer. Displacement was designated as the independent variable for obtaining the other data points.

To obtain the data points for this research a new Method was created for the Instron to follow and apply to all of the specimens. The Method is the set of instructions that the Instron follows to acquire the tensile data, and includes the unit system, selected data types for collection, data acquisition rate, preload, testing load, and number of specimens, among other options. The manual for creating this Method as a new Method is included in the Appendix of this research. The primary values of the Method include applying a preload tensile displacement of 0.125 mm/s (0.005 in/s) until a load of 22.24 N (5 lbf) was applied to the specimen at which point it began ramping the displacement at 0.25 mm/s (0.01 in/s) and measured the required force and strain caused by the displacement. This continued

until the termination criterion of the current force measurement equaling 40% of the prior measurement, a situation that should only occur at fracture.

After an original Method has been made according to the procedure in the Appendix, the process for running subsequent tensile tests proceeds according to the following set of instructions:

1. Be properly dressed per your lab's requirements and have your Personal Protection Equipment (PPE)
2. Turn on the Instron and the attached monitor
3. Create a new folder in the computers file system for the data to be collected
4. Start the Bluehill Universal software
5. Click on and enter the Test section of the Bluehill software
6. Select the original/previous test Method in the new sample section
7. Press OK on the Set Travel Limits page
8. Once the test method has initialized, switch to the Method section
9. Make any changes that are appropriate for your new test such as…
    - Designating the new file to save results to in the exports section
    - Altering the name of the saved results to differentiate the new test in the exports section
    - Designating a new number of samples in the workflow section
    - Others as appropriate
10. Click the Save option and alter the save location to the folder made for the new Method and Change the name of the Method to differentiate the new Method from prior Methods

11. Save the new Method
12. Click on the home button in the top left
13. Do not overwrite the original/previous Method
14. Enter the Test section again
15. Select the new test Method
16. Set the travel limits and press OK
17. Check the Method section to make sure all of the settings meet your desired requirements/parameters
18. Return to the Test section of the sample
19. Select the before test step of the Test process
20. Measure your specimen if you have not as of yet
21. Unlock the loading frame via the unlock button on the console, and raise the crosshead to a height that allows your specimen and a level to fit comfortably between the grips vertically
22. Mount the specimen by inserting the specimen into the upper grip and using a level to ensure that the specimen is aligned vertically before tightening the upper grip.
23. Lower the upper grip and insert the specimen into the lower grip, tighten the lower grip to ensure that the specimen is locked in place as can be seen in Figure 5 below.



Figure 5: A mounted specimen

24. Attach the extensometer to the center of the specimen as can be seen in Figure 6 below.

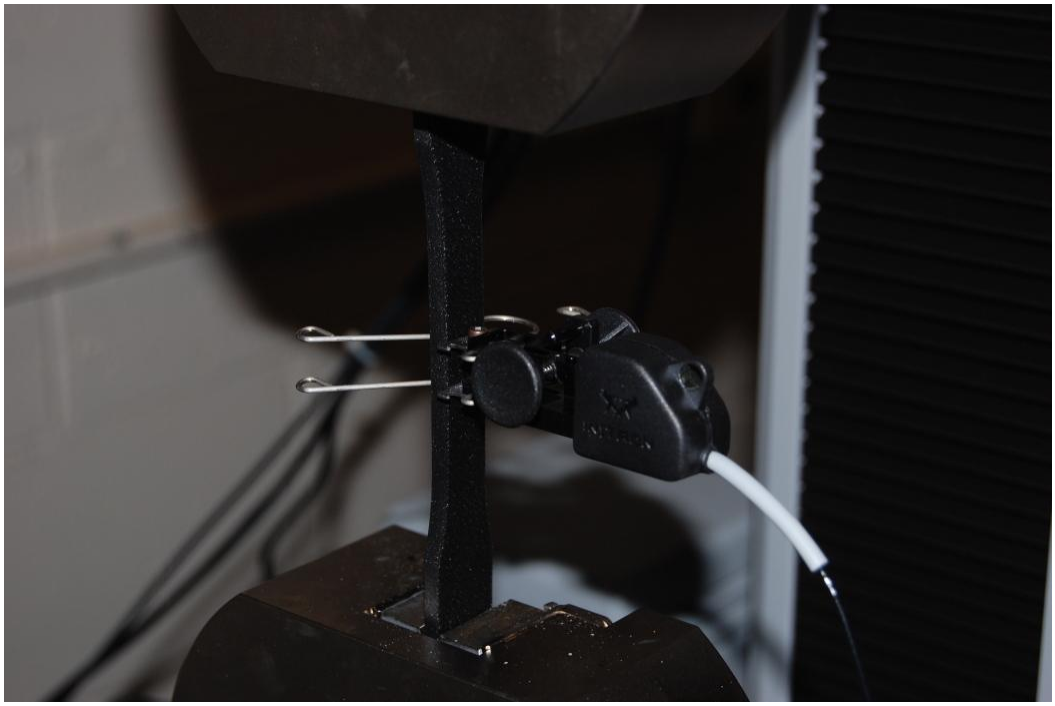

Figure 6: Extensometer attached to a mounted specimen

25. Zero and balance the force, displacement and strain measurements
26. Double check that the specimen has been measured, the clamps are tightened, the Extensometer is on and centered properly, and that your data to be measured are zeroed and balanced
27. Begin the tensile testing of the mounted specimen by pressing the unlock button on the console once more and hitting the start button before the lock reengages
28. Wait for the tensile test to finish and the specimen to fracture
29. Remove the fractured specimen parts from the grips
30. Select the next steps of the testing process to see the generated plots and continue until you are at the page to start the next specimen's tensile test
31. Repeat from step 20 of this process for each specimen of the tensile series

32. Click the checkered flag once tensile testing has been performed on each specimen of the tensile series to finish the tensile testing
33. Save the tensile testing results
34. Check to make sure that the data was added to the destination folder properly
35. Transfer the data to a storage method of your preference
36. Exit out of the Bluehill Universal program
37. Shutdown the monitor and turn off the loading frame

The tensile testing data obtained from the above process was saved as a CSV file to the designated folder by the Bluehill Universal software, and can be opened using the Microsoft Excel Program. The data were copied to a new Excel file so as to maintain the original data file in its unedited form. Using this copied data, stress strain curves for each specimen were produced that Young's moduli could be approximated from. These Young's moduli as well as the tensile strength and strain at fracture data points were collected for each specimen and collected in an Excel file for data keeping.

3.2 Data Analysis

A total of 18 specimens, c.f. Table 1, were subjected to tensile testing in accordance to the Method provided in the prior section. The data obtained from the tensile testing process consisted of time in seconds, displacement in millimeters, tensile force in Newtons, and axial strain in percent. For each specimen, a force vs. displacement and strain vs. displacement plot was created to confirm that the two data sets follow the same trend of increasing as the independent value displacement increases. An example of this plot for the Series A 0-degree specimen can be seen below in Figure 7.

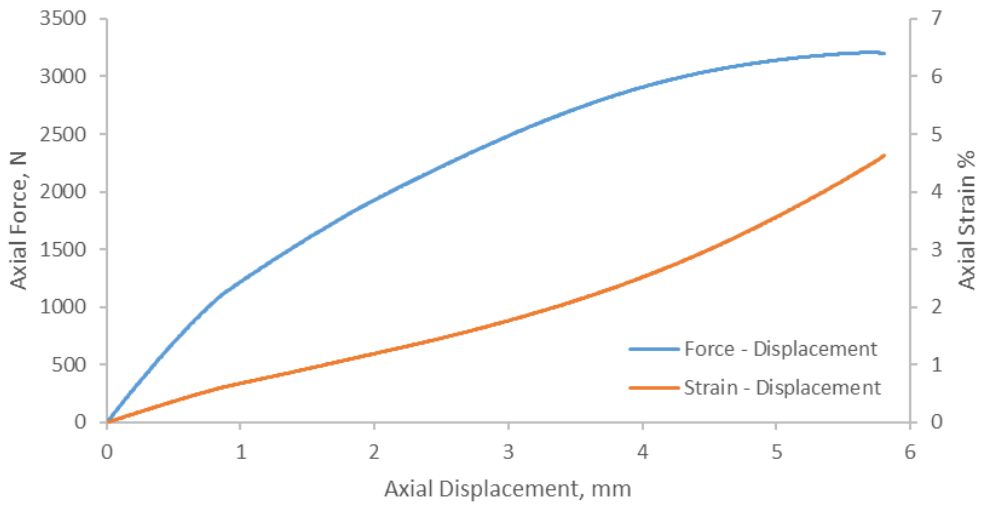

Figure 7:Force and Strain vs. Displacement plot for the A-0 Specimen

This plot shows that as axial displacement increases so too do axial force and axial strain. This makes sense as the force required to consistently increase the displacement should increase, and as the material is stretched to allow this displacement the strain will likewise increase. This plot also shows how while the displacement was increasing at a consistent rate, the force and strain increased at a non-linear rate to the displacement. Similar plots were made for each specimen and can be found in the Appendix and all show the same trend.

With the raw data in hand from the tensile tests, our focus turned to extracting the Young's moduli, tensile strength, and strain at fracture from the raw data. Using the measured values of thickness and width for each specimen from Table 1, tensile stress was calculated using $\sigma = \frac{F}{W \times T}$ where σ is the tensile stress, F is the recorded force, W is the width, and T is the thickness. Along with this modification, the strain was transformed from

the % values that were measured to a simple strain by dividing the percent strain values by 100.

With the calculated stresses and strains in hand, stress-strain curves were made for each specimen. An example of such a curve can be seen below in Figure 8 where the data from the Series A 0-degree specimen is shown.

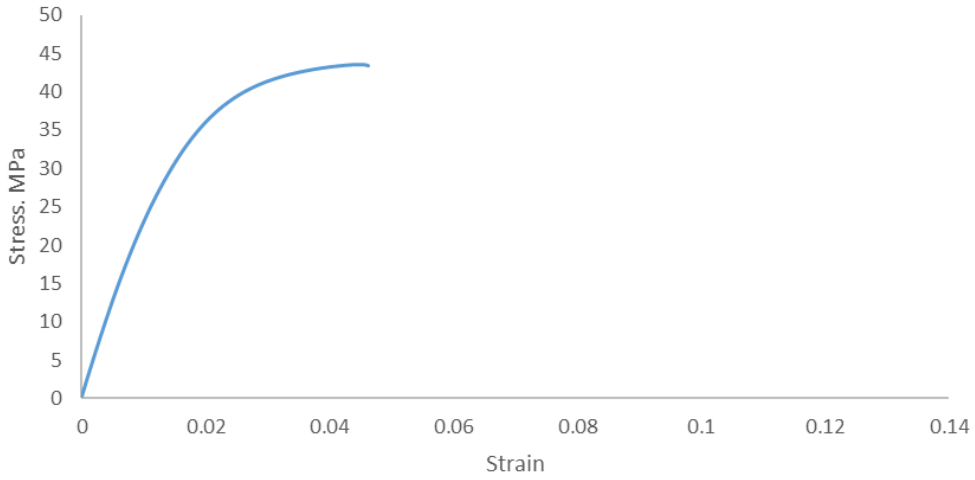

Figure 8: Stress - Strain Response of the A-0 Specimen

Looking at Figure 8, the stress-strain curve looks like what is expected of a stress strain curve. The curve begins at the origin, follows a mostly linear slope to a region where the slope decreases and becomes essentially horizontal until it reaches fracture. Similarly to the Force and Strain vs. Displacement plot previously, the plots of this type for the other specimens can be found in the Appendix.

For each specimen, the initial portion of the stress vs. strain plot that is somewhat linear was extracted by using the first 300 data points of the data set. From these data points a new plot was made, an example of which can be seen below in Figure 9.

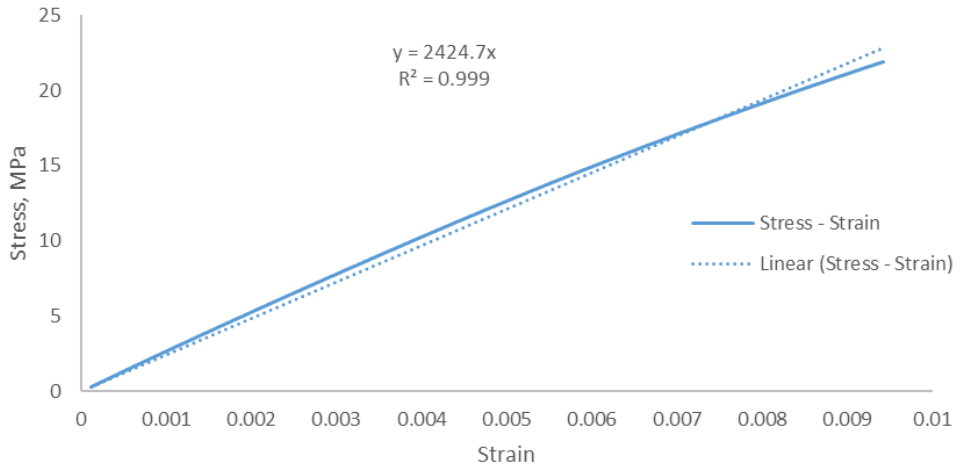

Figure 9: Initial portion of the stress vs. strain plot for A-0

Using Excel's trendline function on the above plot the Young's modulus can be approximated for each specimen along with an R^2 value showing how well the approximated trendline fits the data set. For the linear trendline function the intercept was set to 0. The approximated Young's modulus for a specimen is equal to the slope of the trendline equation of the stress-strain plot. Looking at this plot specifically, the Young's modulus is approximately 2,425 MPa, and the trendline has a strong correlation to the data set of 99.9%. The Young's modulus is rounded from 2,424.7 to 2,425 as the tensile data points collected have decimal points beyond the level of resolution expected of the system. This is in conjunction with the low resolution of the caliper measured width and thickness. As such it was determined that rounding many of the values throughout the obtained results would be appropriate. The plots for the other specimens can be found in the Appendix.

The Young's moduli and their R^2 values for each specimen have been collected in Table 2 below. In addition, Table 2 also contains the tensile strength and strain at fracture for each specimen that were collected from the stress and strain data points by finding the

greatest collected value for each before fracture using the MAX function of Excel. Visual representations of the tensile strength and strain at fracture for an example specimen's plot are shown in figure 10 below.

Table 2: Material Characteristics derived from the tensile tests

Specimen	Young's Modulus (MPa)	Coefficient of determination (R^2)	Tensile Strength (MPa)	Strain at fracture
A-0	2,425	0.999	43.6	0.046
A-45	1,899	0.998	39.5	0.130
A-90	1,726	0.998	36.0	0.063
B-0	2,261	0.998	41.8	0.058
B-45	1,910	0.999	38.6	0.113
B-90	1,806	0.998	35.8	0.076
C-0	2,205	0.998	43.2	0.064
C-45	1,892	0.999	40.2	0.104
C-90	1,753	0.999	38.4	0.081
D-0	2,182	0.998	43.1	0.068
D-45	1,876	0.999	39.5	0.143
D-90	1,708	0.999	36.8	0.093
E-0	3,009	0.999	57.1	0.050
E-45	2,238	0.999	48.6	0.240
E-90	2,138	0.999	47.2	0.146
F-0	2,889	0.999	52.8	0.047
F-45	2,189	0.998	47.8	0.162
F-90	2,280	0.998	45.6	0.143
Average	2133	0.999	43.1	0.102
Std. Dev.	358	$4.97*10^{-4}$	5.7	0.050
Range	1,301	0.001	21.3	0.194

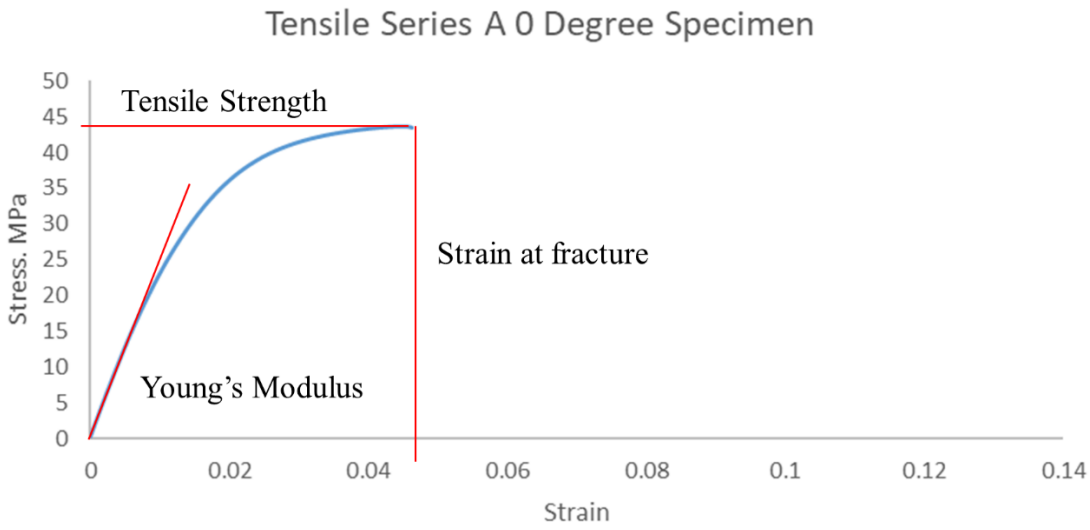

Figure 10: Visual representation of tensile strength and strain at fracture

3.3 Discussion of Results

Using Excel's data selection function, plots were made to compare the stress-strain curves of multiple specimens. Comparison plots were made for each specimen series, each angle, and finally all of the stress vs. strain curves. The first type of comparison plot analyzed in this section compares the stress-strain curves of the three specimens from a specimen series. Figures 11-16 below are this type of comparison plot for series A-F respectively.

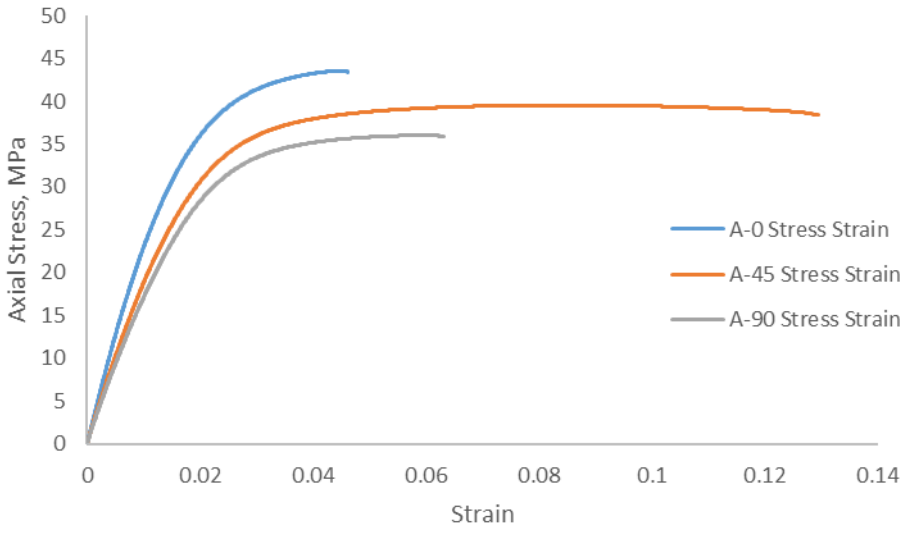

Figure 11: Tensile Series A Stress-Strain Comparison

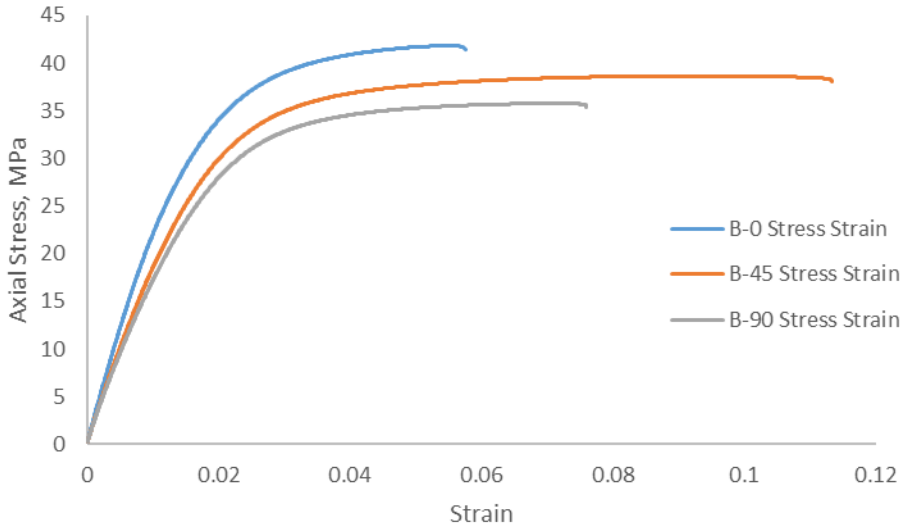

Figure 12: Tensile Series B Stress-Strain Comparison

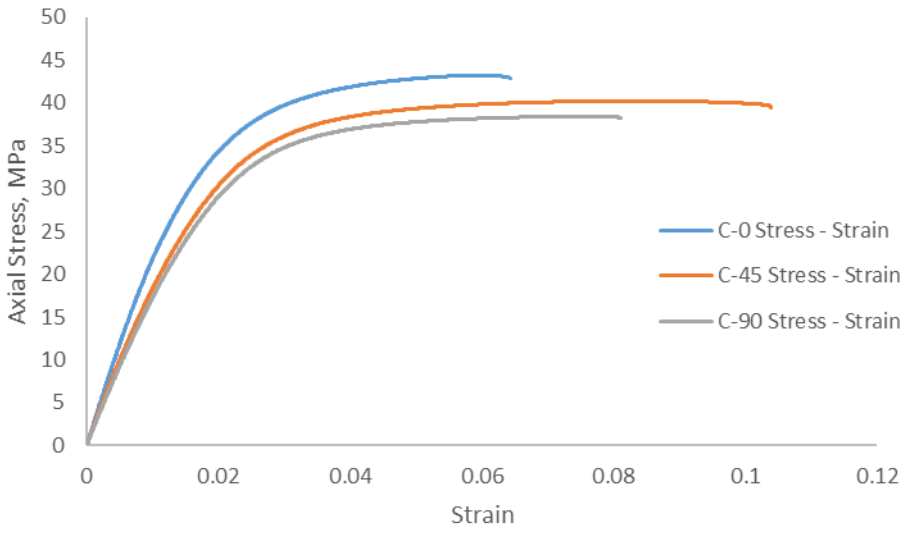

Figure 13: Tensile Series C Stress-Strain Comparison

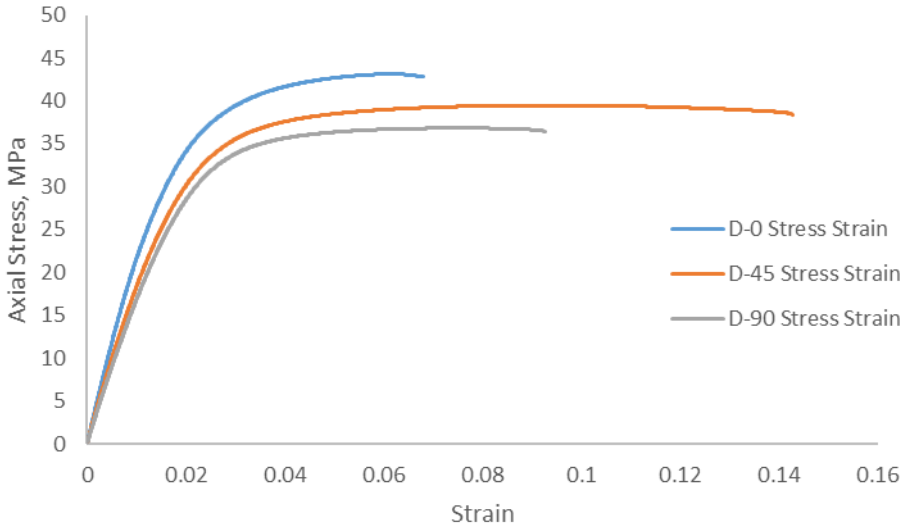

Figure 14: Tensile Series D Stress-Strain Comparison

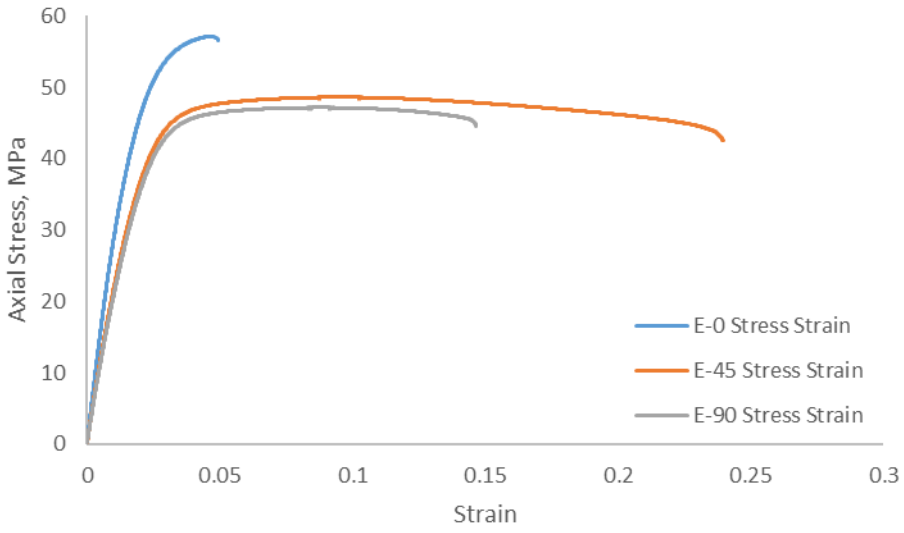

Figure 15: Tensile Series E Stress-Strain Comparison

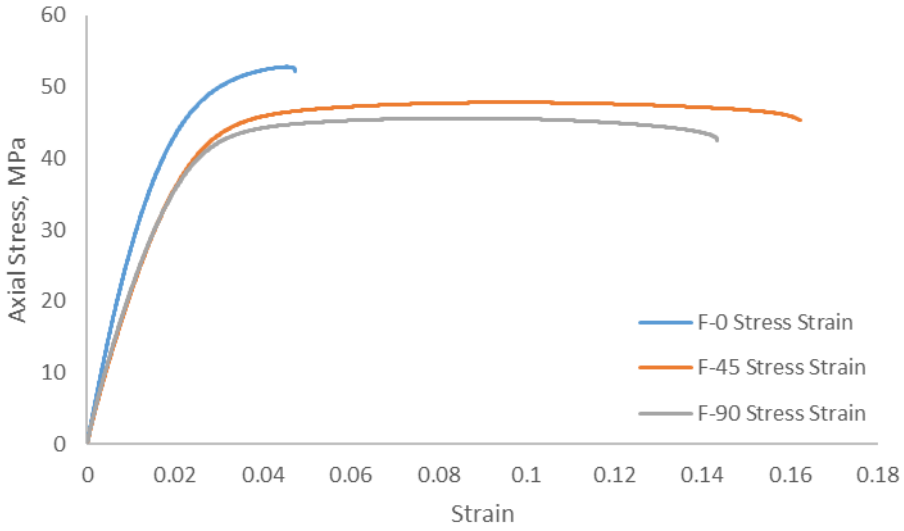

Figure 16: Tensile Series F Stress-Strain Comparison

In these plots there are two primary patterns and one secondary pattern that can be seen to be consistent throughout the different series. The first primary pattern is that the 0-degree specimen consistently has the greatest tensile strength, the 45-degree specimen has the next greatest tensile strength, and finally the 90-degree specimen has the least great tensile strength. An example of this can be seen by looking at the Series A comparison plot

in which the 0º specimen had a tensile strength 10.4% greater than the 45º specimen, while the 45º specimen's tensile strength was 9.7% greater than the 90º specimen's tensile strength. This makes sense on an intuitive level as the material in the 0-degree specimens were in line with the direction the stress was being applied, and as such should be capable of resisting the stress to a better degree than the other specimens. In comparison, the material in the 90-degree specimens is perpendicular to the direction of stress and would be least capable of resisting the stress. The 45-degree specimens therefore fall in the middle as their material is in a state midway between parallel and perpendicular to the stress. The second primary pattern that can be seen in these plots is the pattern of strain at fracture. In this pattern, the 45-degree specimen consistently reaches the greatest strain before fracture, followed by the 90-degree specimen, and the 0-degree specimen consistently fractures at the least strain in comparison to the other specimens of the same series. This can be seen in the Series A comparison plot in which the 45º specimen's strain at fracture is 106.4% greater than the 90º specimen's strain at fracture while the 90º specimen's strain at fracture is 37.0% greater than the 0º specimen. These patterns can also be seen by referring back to Table 2 and comparing the tensile strength and strain at fracture between specimens of a series. Consequently, these patterns show evidence that suggests that the raster angle has noticeable and repeatable effects on the material characteristics of the printed specimens and supports rejecting the first null hypothesis of this research.

The secondary pattern that can be seen in these series comparison plots is that the 0-degree sample tends to be the stiffest specimen. This is based off of the 0-degree specimens having the greatest Young's moduli. Following the 0-degree specimens, the 45-degree specimens have the next greatest Young's moduli, and the 90-degree specimens

usually have the least Young's Moduli. The only point that goes against this pattern, and what made it designated as a secondary pattern, would be the Young's Modulus of F-45 and F-90 where F-45 has a lower Young's modulus than F-90. However, looking at Figure 15 it can be seen that the incline of these two data sets in the linear region is overlapping and F-45 still follows the primary pattern of reaching a greater stress than F-90 before its incline declines out as it enters the non-linear region despite this so it could be due to the range of data selected for estimating the Young's moduli of these two specimens.

The next set of comparative plots that were made compare the specimens that share their raster angle. These plots are shown in the order of 0°, 45°, and then 90° in Figures 17, 18, and 19 respectively.

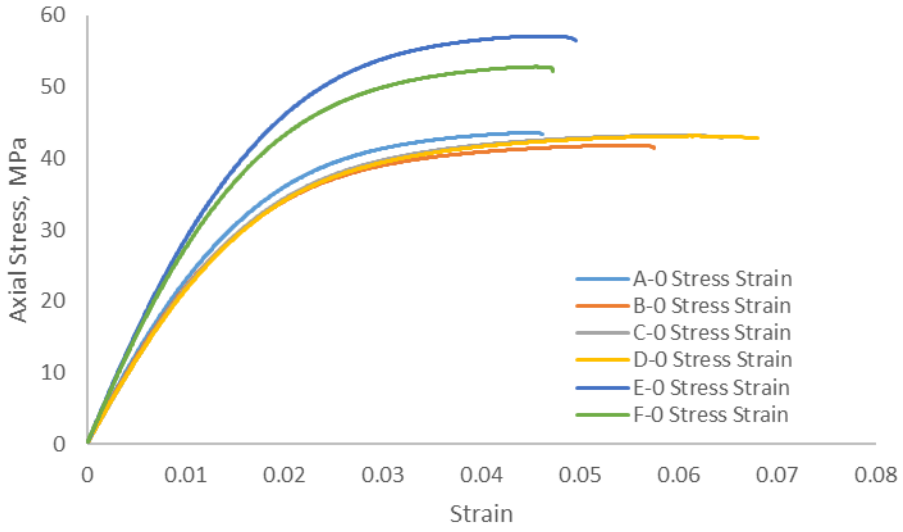

Figure 17: 0-Degree Specimens of Each Tensile Series

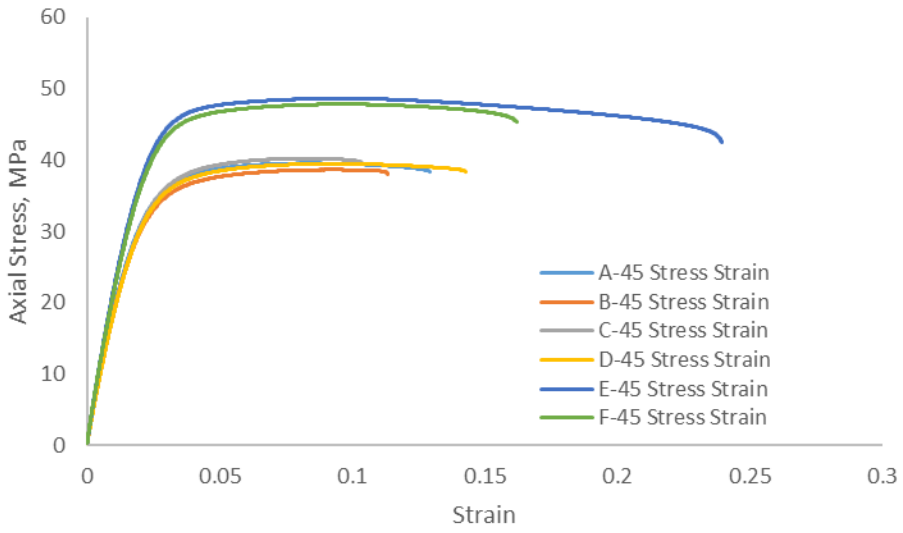

Figure 18: 45- Degree Specimens of Each Tensile Series

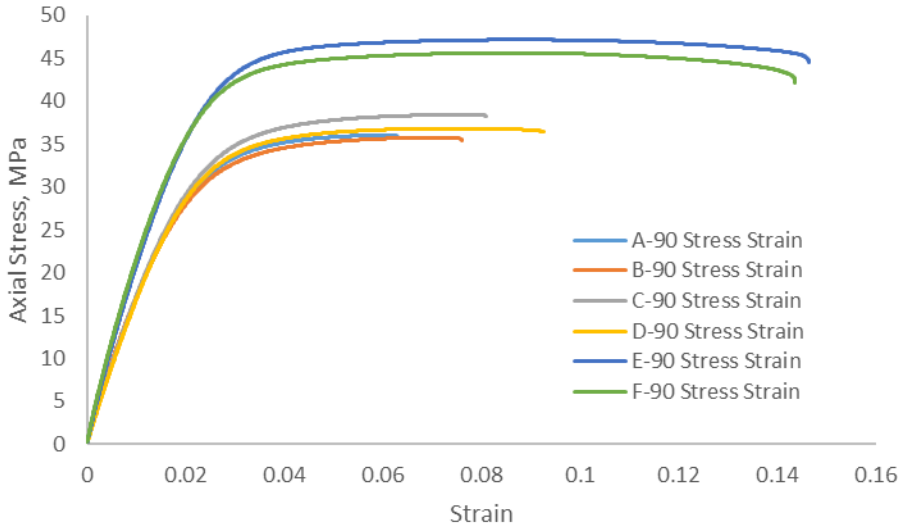

Figure 19: 90- Degree Specimens of Each Tensile Series

Moving the analysis to this next set of plots, the angle specific plots also have a point of interest. In these plots it can be seen that the specimens have split into two groups of A-D and E-F. These groupings are designated primarily by the incline of the specimens in their linear region as each specimen tends to become more unique as they enter their

non-linear regions. This splitting into groups is a point of interest as the material that was used for producing each specimen was the same, yet E-F are shown to reach greater stresses before fracture regardless of raster angle. The reason for this occurring is unknown as of now, as the only primary difference between A-D and E-F is that E-F were produced earlier on in the process of this research. However, despite the difference in the max stress between the two group, all of the tensile series still follow the patterns that were previously mentioned. This shows that despite the seeming difference in mechanical properties, the raster angle is still affecting the material in the same way, and is supporting evidence that the angle of print does have an effect on the final mechanical properties of a specimen.

The final plot made for comparing the stress-strain curves of specimens compares the stress-strain curves of every tensile specimen in one plot and can be seen in Figure 20 below.

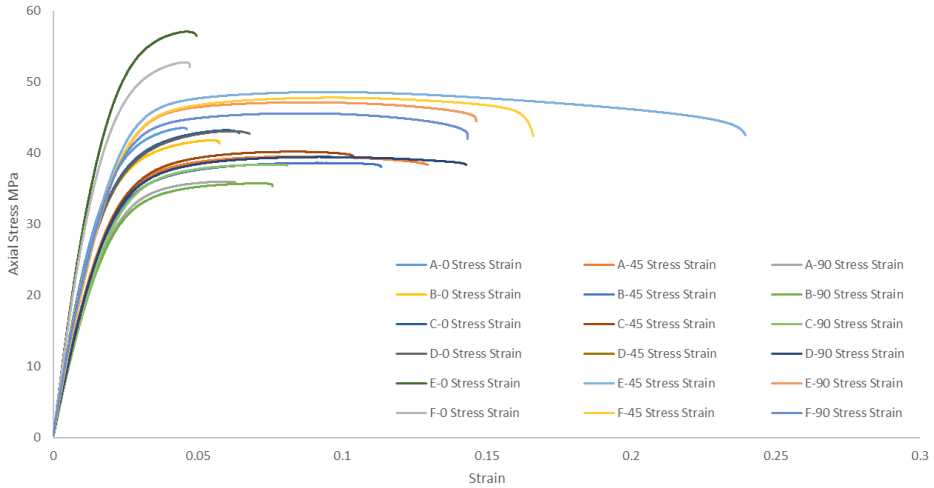

Figure 20: A collection of the tensile data for every specimen

Looking at the results in Figure 19 of the total collection of stress vs. strain curves, a number of comparisons become more obvious than when looking at individual stress-

strain curves or the comparison curves for individual series or angles. The first of these points would be to observe just how much greater the tensile stress of E-0 and F-0 is to every other specimen. Still looking at the results of series E and F, it can be seen in this plot that E-90 and F-90 which have the lowest tensile strength of the E and F series have greater tensile strengths than the 0-degree specimens of series A-D. However, moving on from the differences between E and F with the other series it can be seen in this plot how distinct the results are when comparing the specimens of different angles for series A-D. This can be seen in how distinct the grouping for specimens of angles is in the plot, supported by there being no overlap between the 0°, 45°, or 90° specimens of series A-D.

The final point of discussion for the results of this chapter is the comparison of the values from Table 2 with the reported values of the material when purchased. To restate the pertinent mechanical properties stated by the vendor, this material is reported to have a Young's modulus of 6,000 MPa, and Tensile strength of 100 MPa. However, based on the results from tensile testing the greatest Young's modulus found in the tested specimens was 3,009 MPA for the E-0 specimen, while the greatest Tensile strength of 57.1 MPa was also observed in the E-0 specimen. While it does make sense that the specimen with the greatest Young's modulus would also have the greatest Tensile strength, the fact is that both values are only slightly greater than half of the values that the vendor stated. This is especially relevant as E-0 had a greater tensile strength to the point that it was visually obvious when comparing it to the other 0-degree specimens that were tested. The 0-degree specimens of series A-D tended to have tensile strengths closer to the 43 MPa region which do not even reach half of what the vendor states to be the expected tensile strength of this material. The cause of this difference is not known as of now.

Chapter 4: Specimen Prep for Microscopy

This Chapter's focus is on the process and results of making and polishing molds of the gage-lengths of specimens in preparation for performing microscopy on the molded specimens.

4.1 Molding

In addition to collecting data through tensile testing, microscopy data was also collected for this research. To prepare specimens for microscopy, the specimens were set in a mold made of Allied Quickcure. To start this process, the gage lengths of specimens were debrimmed and bisected horizontally so that there was access to the internal cross-section of the specimens and that they would fit into the mold cups. For this research, the bisecting step was completed using a Dremel tool attached with a metal cutting head attachment.

After the gage length halves cooled down from the cutting process, and were cleaned, a mold cup (Struers Product ID 40300089) was designated for each specimen to be molded in, and the following process was followed to make molds of the specimens:

1. PPE is worn, including lab coat, gloves, and eye protection.
2. The molding process begins by adding Allied Quickcure reagents (Allied Product ID 170-10000) at a ratio of 2:1 of solid and liquid reagents respectively into a designated mixing cup and stirring the solution until it is thoroughly mixed and in the form of a viscous fluid.
3. The mixed solution is poured slowly into the bottom of a mold cup until the bottom of the mold cup is covered with a thin layer of the solution of approximately 2 mm.

a. While the bottom of the mold cup is being filled, the mold at this end will be considered the top of the mold itself throughout this research as this is the side that will be viewed for microscopy after the molding and polishing processes are complete. Similarly, the end of the mold at the top of the mold cup will be considered as the bottom of the mold.

4. After covering the bottom of the mold cup with the solution, one of each bisected gage length for a specimen series is placed vertically into the mold cup, cut end at the bottom of the mold cup, according to the pattern shown in Figure 21 below. This pattern is used consistently through every mold to keep track of which gage length is what angle as the mold makes it difficult to see the side of the gage lengths clearly and removes sharpie-based markings on the gage lengths.

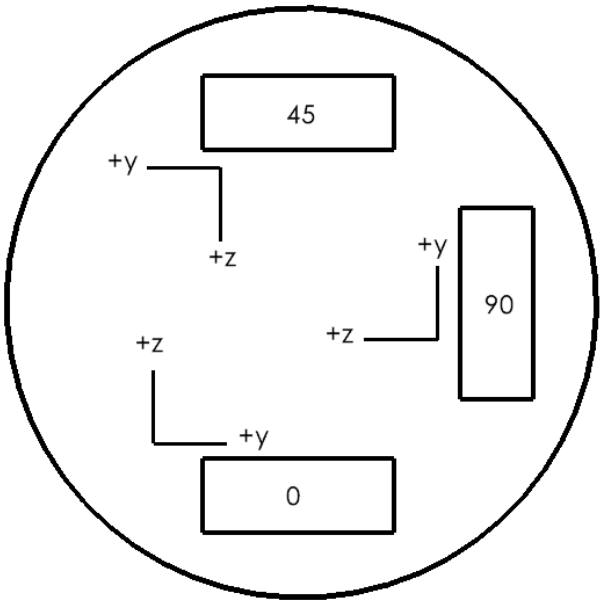

Figure 21: Orientation of specimens in mold

5. Once the gage lengths are in the mold cup according to the designated pattern, the remainder of the mold cup is slowly filled with more of the fluid while taking care to not disturb the gage lengths and repositioning them if they are disturbed in the process.
6. Once the mold cup is filled and the specimens are fully covered the mold is allowed to sit and settle for twenty-four hours to guarantee it has set fully.

After allowing the mold to set, it was removed from the mold cup, and polished using a Struers Laboforce 3 Semi-automatic Polisher shown below in Figure 22.



Figure 22: Struers Polisher

To polish the molds, the following process was used:

1. PPE is worn, including a lab coat, gloves, and eye protection.
2. A magnetic plate with a textured top side is first mounted and wetted by running water over the plate as the polisher runs to spread a thin layer evenly across the plate.
3. This is followed by removing the water while the polisher continues to run.
    a. This is done because the 800-grit sandpaper that is to be mounted does not have an adhesive side to help it stick to the textured plate.
4. With the textured plate mounted and wetted, a sheet of 800-grit sandpaper (Struers Product ID 40400010) is mounted on the polisher over the textured plate.
5. The sandpaper is then wetted in the same way that the textured plate was wetted.

6. With the 800-grit sandpaper mounted and wetted, the mold is locked into place in the instrument, bottom down, and the screw is tightened until the indicator reads between the second and third marks from the bottom.
7. After locking the mold into place, water is continuously run over the plate as the instrument is repeatedly turned on for one-minute intervals to remove the rough edges and irregularities that were often present after the molding process.
    a. Between each one-minute run of the polisher the screw is checked to make sure that it is still within the accepted range.
8. Once the irregularities are removed from the bottom of the mold, it can be dismounted from the instrument and washed off to remove any remnant material from the sandpaper.
9. The 800-grit sandpaper is then removed, and replaced with a 1000-grit sandpaper (Buehler Product ID 36081000) by pulling the tab on the side of the 1000-grit sandpaper and removing the cover from the adhesive side of the sandpaper to securely mount it to the instrument.
10. The 1000-grit is then wetted like with the 800-grit sandpaper.
11. With the 1000-grit sandpaper mounted and wetted, the mold can be mounted into the polisher once more, with the top down this time.
12. The polisher is then run for 15 one-minute intervals, while checking that the screw is between the second and third marks from the bottom each time.
    a. While the bottom of the mold can take several repetitions of the one-minute intervals, the process that was determined for the top of the

mold was to run it through 15 one-minute intervals for each of the polishing materials.

13. After running the top of the mold over the 1000-grit sandpaper for 15 one-minute intervals, the mold can be dismounted and rinsed off once more.
14. The 1000-grit sandpaper is then replaced with a 1200-grit sandpaper (Allied Product ID 50-10077) that is also mounted via its adhesive layer before wetting it.
15. With the 1200-grit sandpaper mounted and wetted, the mold can be mounted and secured by tightening the screw once more before starting the next 15 one-minute intervals.
16. Once the 15 1200-grit intervals are run, the mold can be dismounted and washed off again, making sure to lay the mold bottom down so as not to get anything on the top of the mold or scratch it, and the 1200-grit sandpaper sheet can be removed from the instrument.
17. With the 1200-grit polishing completed, the magnetic plate is removed, and the instrument can be prepped for the 3- and 1-micron treatments.
    a. To prepare for this, the 3- and 1-micron polishing suspensions had already been transferred into empty and sterilized containment bottles connected to a Struers Labodoser, pictured in Figure 22 above, that allowed for controlled distribution of the suspensions to be dispensed onto the plate.
18. Before mounting the mold this time, a MD-Dur plate (Struers Product ID 40500074) is mounted and prepped by running the polisher with the 3-

micron suspension selected on the Labodoser until the 3-micron polishing suspension (Struers Product ID 40600535) begins to be dispensed onto the plate.

19. The polisher is then mounted with a washed, blank mold to spread a fresh layer of the suspension across the plate evenly.
    a. If this is the first time polishing, the plate will be blank, otherwise the plate previously used for 3-micron polishing will be used so as to keep the polishing suspensions from being mixed.
20. After evenly spreading the 3-micron suspension over the plate, the blank mold can be removed and washed, and the specimen mold can be mounted top-down in the instrument and ran for 15 one-minute intervals while selecting for the 3-micron suspension each time the instrument is started.
21. After these 15 intervals of polishing with the 3-micron polishing suspension, the mold is dismounted and washed off to remove any remnants of the polishing suspension from the face being polished.
22. The 3-micron plate is then removed from the instrument and stored for future use, and the next plate is prepped in the same way as the 3-micron plate except selecting for the 1-micron suspension.
    a. Similarly to the 3-micron plate, if this is the first time prepping for the 1-micron suspension a blank plate will be used, otherwise the 1-micron plate from prior polishing sessions will be used.
23. After prepping for the 1-micron suspension (Struers Product ID 40600555) by evenly spreading it out across the plate with a washed blank mold, the

specimen mold can once more be mounted into the instrument top down and ran with the 1-micron suspension for 15 one-minute intervals.

24. After finishing this set of 15 intervals, the mold can be dismounted and washed off once more before it is stored in preparation to be transported to the location where microscopy will be performed on it.
    a. Along with storing the mold, the 1-micron plate is removed from the instrument and stored in a similar way to the 3-micron plate for future use.
25. The polishing station is then cleaned and left in a ready state for the next person who will use it.

4.2 Results

The results of molding and polishing the gage lengths for each specimen of each set is best expressed in an image of the finalized, polished molds. Below is Figure 23, an image of the six molds that were produced and polished. Each mold contains approximately half of a gage length of each angle for its series.



Figure 23: The Six Molds in the Order A, B, C, D, E, and F

Chapter 5: Microscopy

This chapter's focus is on how microscopy was performed on the polished molds from Chapter 4 and discusses the conclusions drawn from the images obtained from this microscopy.

5.1 Imaging Procedure

After polishing the molds, the next step was to begin microscopy. To start this process, a time was reserved at the Samuel Roberts Noble Microscopy Lab on the University of Oklahoma campus through the Agilent Cross Lab website ilabsolutions.com for the Keyence VHX-7000 ultramicroscope. Once there, the microscope and its associated computer were turned on and initialized. The mold was removed from its storage container and placed centrally on the microscope's viewing plate, and the full ring lighting was chosen from the lighting options. From this point, the microscope was controlled via the computer to find points of interest on the specimen within the mold. For each point of interest, the microscope was focused before capturing a set of images at three magnifications at that point, refocusing the microscope between each capture. During microscopy, the viewing plate was rotated to ensure that the z-axis of the specimen was in line with the vertical of the captured images and the x-axis was aligned to be coming out of the image. The magnifications captured in this research were 100x, 200x, and 500x. Photos were taken of a point of interest from each specimen at these magnifications in both .jpg and .tif formats.

5.2 Discussion of Results

In total, the number of microscopy images taken were 54 for each file format. From these images, three have been chosen to show as examples, one for each angle that

gives the best view of the state of the carbon fibers in that specimen. These examples constitute Figures 24-26 below.

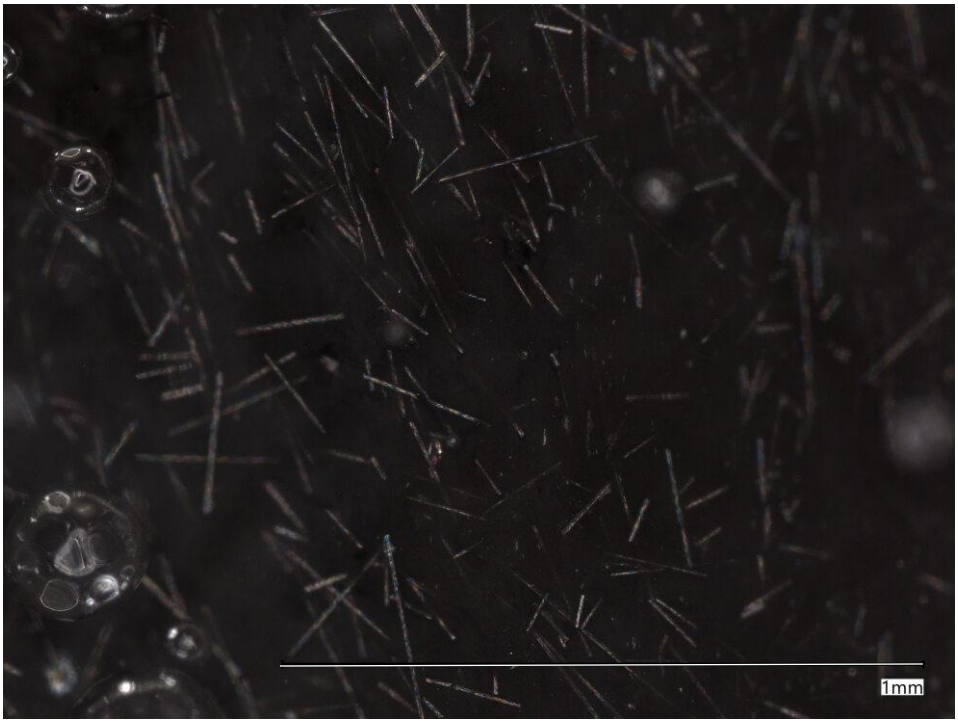

Figure 24: Specimen C-0 at 200x magnification

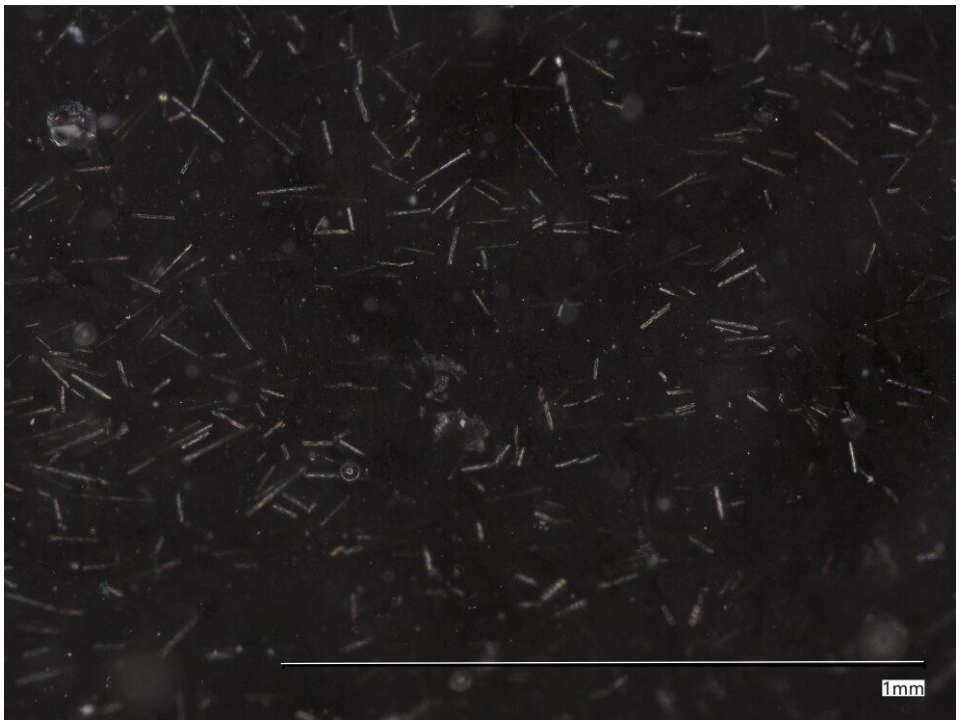

Figure 25: Specimen B-45 at 200x magnification

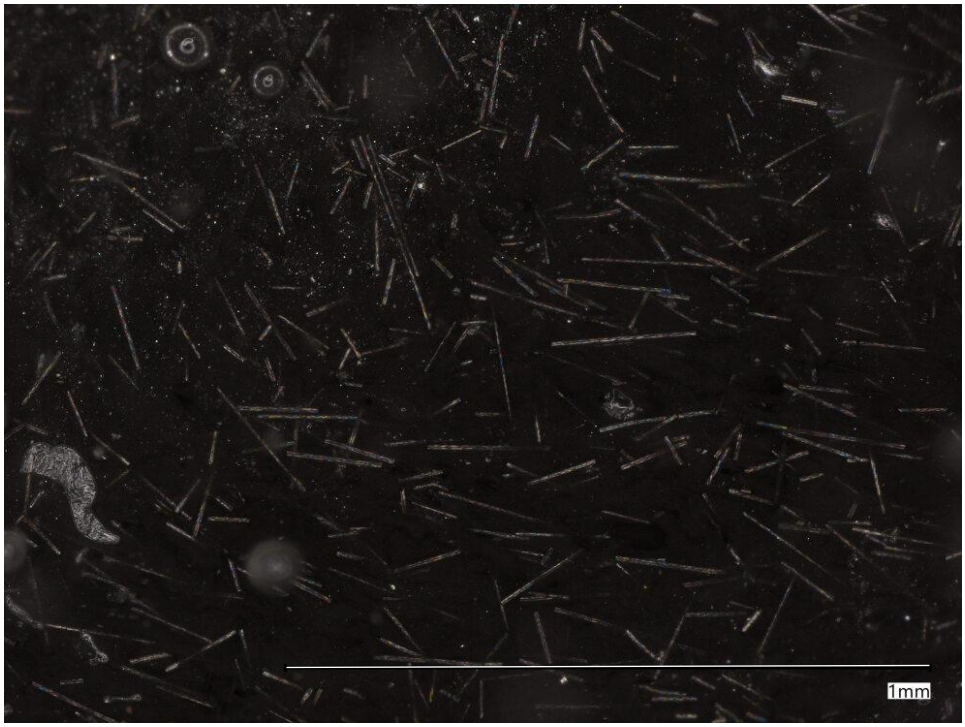

Figure 26: Specimen D-90 at 200x magnification

Looking at Figures 24-26, the thin white lines were determined to be the carbon fibers dispersed throughout the specimens. While no statistical analysis was performed, the distribution of the carbon fibers was deemed to be mostly unaffected by the raster angle of the specimen. This conclusion was reached, as regardless of which specimen's microscopy image was looked at, there did not appear to be any reliable way to differentiate which raster angle specimen was being examined. This was deemed to mean that all three angles of specimens appear similarly unorganized. If the carbon fiber distribution is similarly unorganized regardless of angle, this can be used to assume that it is unlikely that the carbon fibers are having a considerable effect on the material characteristics based on the specimen's raster angle. This seeming randomness of the carbon fibers also allows for the material to be assumed as somewhat isotropic for the sake of material characterization. These results, while not statistically supported, appear to stand as evidence that the raster angle does not have a noticeable effect on the orientation of the fibers in the specimens. This supports failing to reject the second null hypothesis of this research.

Chapter 6. Concluding remarks

6.1 Interpretations

In summary, in Chapter 3 it was determined that based on the results obtained in this research, the material characteristics follow two primary patterns and one secondary pattern as a function of the raster angle of the specimen. The first primary pattern is in regard to the tensile strength that the specimens reached. In this pattern, it was observed that the 0-degree specimens consistently reached the greatest tensile strength, the 45-degree specimens reached the next greatest tensile strength, and the 90-degree specimens reached the least great tensile strength. An example of this was shown when comparing specimens of Series A in which the 0º specimen had a tensile strength 10.4% greater than the 45º specimen, while the 45º specimen's tensile strength was 9.7% greater than the 90º specimen's tensile strength. The second primary pattern was in regard to the strain at fracture that the specimens would reach. In this pattern it was determined that the 45-degree specimen consistently reached the greatest strain at fracture, the 90-degree specimen reached the next highest strain at fracture, and the 0-degree specimen reached the least great strain at fracture. This was shown in the comparison of Series A in which the 45º specimen's strain at fracture was 106.4% greater than the 90º specimen's strain at fracture while the 90º specimen's strain at fracture was 37.0% greater than the 0º specimen.

The secondary pattern that was observed in the tensile results was that the 0-degree specimen was typically the stiffest based on it consistently having the greatest Young's modulus of the series, the 45-degree specimen being the next stiffest based on its Young's modulus, and the 90-degree specimen being the least stiff. This pattern is considered as secondary, as while it held for the majority of specimen series, the F series had its 45 and

90-degree specimens switch according to their Young's moduli. It was determined that this could be a problem of chosen data points to create the Young's moduli estimates as the two specimens' Young's moduli were very close and overlapping in the plot of the F series.

The primary patterns in the tensile results showed that there was evidence that the raster angle had a noticeable and repeatable effect on the tensile properties of the printed specimens. This evidence supports rejecting the first null hypothesis of this research.

In Chapter 5, it was deemed that upon observation of the microscopy images the carbon fibers did not appear to follow any angle-based patterns. Given this finding, it could be assumed that it was unlikely that the fibers were giving any considerably greater reinforcement to one angle over another. It was also assumed, based on the lack of pattern, that the specimens were mostly isotropic for the sake of material characterization.

The findings from Chapter 5's results show that the fibers appear to be quasi-randomly oriented regardless of raster angle. These results support failing to reject the second null hypothesis of this research.

These results agree with the findings of the paper by Ning et al. [11] referenced in Chapter 1 where they also found a difference based on raster angle. However, in comparison, the data from this research shows that while they found their (0,90) specimens to have the greatest tensile strength it was likely that the 0-degree layers of their samples were contributing the majority of the tensile strength in those results. This shows that if the stress direction is known for a structural member the greatest tensile strength will be achieved by aligning the raster angle with that stress direction. Similarly, if the expected high strain direction is known, and strain is the characteristic that needs to be built for,

aligning the raster angle 45° with the direction of strain provides the greatest strain before fracture. Given this information, depending on the requirements for a part, it can also be proposed that, as 45° specimens had the second greatest tensile strength and the greatest strain at fracture, aligning the raster angle 45° to the direction of expected stresses will produce a structure that will have a marginally lesser tensile strength than a 0° raster angle structure while being able to withstand the most strain.

6.2 Plans for the future

Given the results that were obtained in this research there are primarily three different directions that could be studied to continue this route of investigation.

1. First, conduct studies to investigate the effects of a wider range of angles such as 15°, 30°, 60°, and 75° and see how the results compare to the results found in this research.
2. A second possible expansion would require a larger experimental program. This point would be to essentially repeat this round of research, but instead of using only one material for the research using a variety of materials to see if the patterns that were discovered in Chapter 3 hold regardless of material.
3. The third expansion method would focus on the microscopy and image analysis side of this research by performing a more detailed analysis, such as including statistical calculations.

References

[1] Additive Manufacturing Market Size Report, 2030. (n.d.). https://www.grandviewresearch.com/industry-analysis/additive-manufacturing-market

[2] González, C. M. (2020, January 30). *Timeline of the 3D printing history*. ASME. https://www.asme.org/topics-resources/content/infographic-the-history-of-3d-printing

[3] Birosz, M. T., Andó, M., & Ledenyák, D. (2021a). Effect of FDM infill patterns on mechanical properties. SSRN Electronic Journal. https://doi.org/10.2139/ssrn.3950131

[4] Plocher, J., Wioland, J.-B., & Panesar, A. S. (2022). Additive manufacturing with fibre-reinforcement – design guidelines and investigation into the influence of infill patterns. Rapid Prototyping Journal, 28(7), 1241–1259. https://doi.org/10.1108/rpj-09-2021-0223

[5] Abderrafai, Y., Hadi Mahdavi, M., Sosa-Rey, F., Hérard, C., Otero Navas, I., Piccirelli, N., Lévesque, M., & Therriault, D. (2022). Additive manufacturing of short carbon fiber-reinforced polyamide composites by fused filament fabrication: Formulation, manufacturing and characterization. *Materials & Design*, *214*, 110358. https://doi.org/10.1016/j.matdes.2021.110358

[6] Russell, T., & Jack, D. A. (2023). Tensile and compression strength prediction and validation in 3D-printed short-fiber-reinforced polymers. Polymers, 15(17), 3605. https://doi.org/10.3390/polym15173605

[7] Wang, K., Li, S., Rao, Y., Wu, Y., Peng, Y., Yao, S., Zhang, H., & Ahzi, S. (2019). Flexure behaviors of ABS-based composites containing carbon and kevlar fibers by material extrusion 3D printing. Polymers, 11(11), 1878. https://doi.org/10.3390/polym11111878

[8] Nawafleh, N., Elibol, F. K., Aljaghtham, M., Oflaz, E., Ciciriello, A. J., Dumont, C. M., Dauer, E., Gorguluarslan, R. M., Demir, T., & Celik, E. (2020). Static and dynamic mechanical performance of short kevlar fiber reinforced composites fabricated via direct ink writing. Journal of Materials Science, 55(25), 11284–11295. https://doi.org/10.1007/s10853-020-04826-w

[9] Banjanin, B., Vladic, G., Pál, M., Balos, S., Dramicanin, M., Rackov, M., & Knezevic, I. (2018). Consistency analysis of mechanical properties of elements produced by FDM Additive Manufacturing Technology. Matéria (Rio de Janeiro), 23(4). https://doi.org/10.1590/s1517-707620180004.0584

[10] Wang, J. Y., Xu, D. D., Sun, W., Du, S. M., Guo, J. J., & Xu, G. J. (2019). Effects of nozzle-bed distance on the surface quality and mechanical properties of fused filament fabrication parts. IOP Conference Series: Materials Science and Engineering, 479, 012094. https://doi.org/10.1088/1757-899x/479/1/012094

[11] Ning, F., Cong, W., Hu, Y., & Wang, H. (2016). Additive manufacturing of carbon fiber-reinforced plastic composites using fused deposition modeling: Effects of process parameters on tensile properties. Journal of Composite Materials, 51(4), 451–462. https://doi.org/10.1177/0021998316646169

Appendix

Appendix 1: Creating an Instron Test Method

The process for creating a new Method from scratch follows these steps:

1. Turn on the Instron and attached monitor
2. Create a new folder that will be where you will save the new method
3. Start the Bluehill Universal program
4. Enter the test section and choose the create a new method option in the new sample section
5. Choose tension method
6. Press OK on the set the travel limits page
7. Save the method to the folder that you made for it
8. In the General section
    a. Set system of units to SI
    b. Set specimen parameters to method default
9. In the sample section
    a. Make no changes
10. In the Specimen section
    a. In the Properties section, modify the geometry based on the specimens
11. In the Measurements section
    a. Add Strain from the Measurement types to Measurements available in the method
12. In the Calculations section
    a. Make no changes
13. In the Test Control section

a. In the strain section, set the primary source to Strain 1
b. In the pre-test section:
    i. Turn pre-load on and set the rate to 0.125 mm/s
    ii. Set the changeover criteria measurement to Force and set it to 22.24 N
c. In the Test section, set control mode to displacement and set it to 0.25 mm/s
d. In the end of test section:
    i. Set criteria 1 to measurement rate
    ii. Set measurement 1 to force
    iii. Set sensitivity 1 to 40%
    iv. Set End of test action to stop
e. In the Data section:
    i. Set capture scheme to custom settings
    ii. Set measurement 1 to Time
    iii. Set interval 1 to 20 ms

14. In the Console section
    a. Add Strain 1 and Time to selected live displays
    b. Set the order of the live displays to be Time, Displacement, Force, Strain 1
15. In the Workspace section
    a. Turn gridlines off for both graph 1 and 2 in their advanced sections
    b. On Graph 2 set the Y-Data to be Strain 1
    c. In the Raw Data section add Strain 1 to the selected measurements

16. In the Exports Section
    a. In the File settings section
        i. Add the file you created for this method as the file location
        ii. Modify the sample file name to be recognizable for the test
    b. In the exports 1 and 2 sections set the frequency to at finish
    c. In the exports 1 section set raw data to on
17. In the workflow section
    a. Set the number of specimens to the number in a series
    b. Turn run as prompted test on
18. In the reports section
    a. In the body section, add graph 2 and results 2 to the selected items
19. Save the method

Appendix 2: Force-Displacement and Strain-Displacement Results

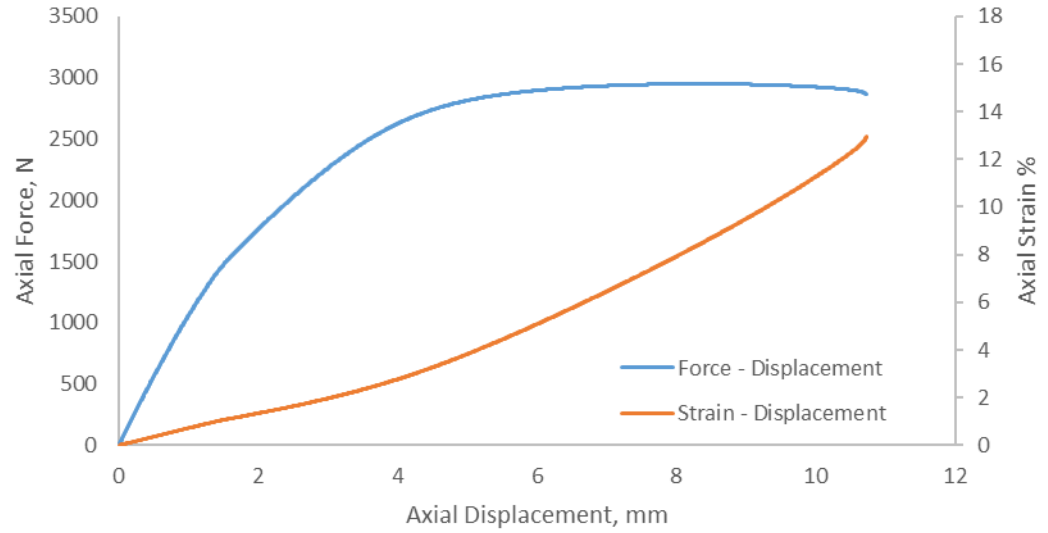

Figure 27: Force & Strain vs. Displacement for A-45

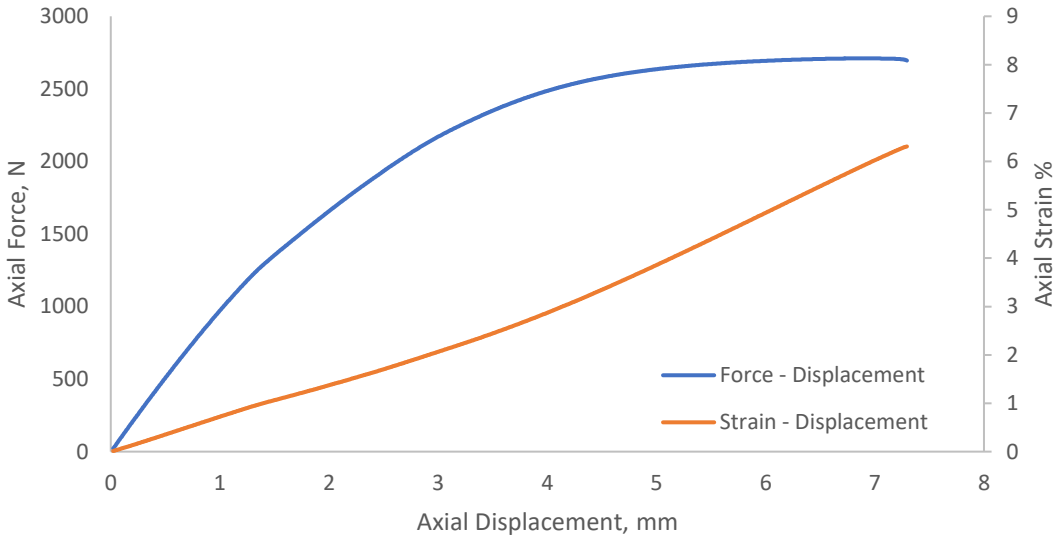

Figure 28: Force & Strain vs. Displacement for A-90

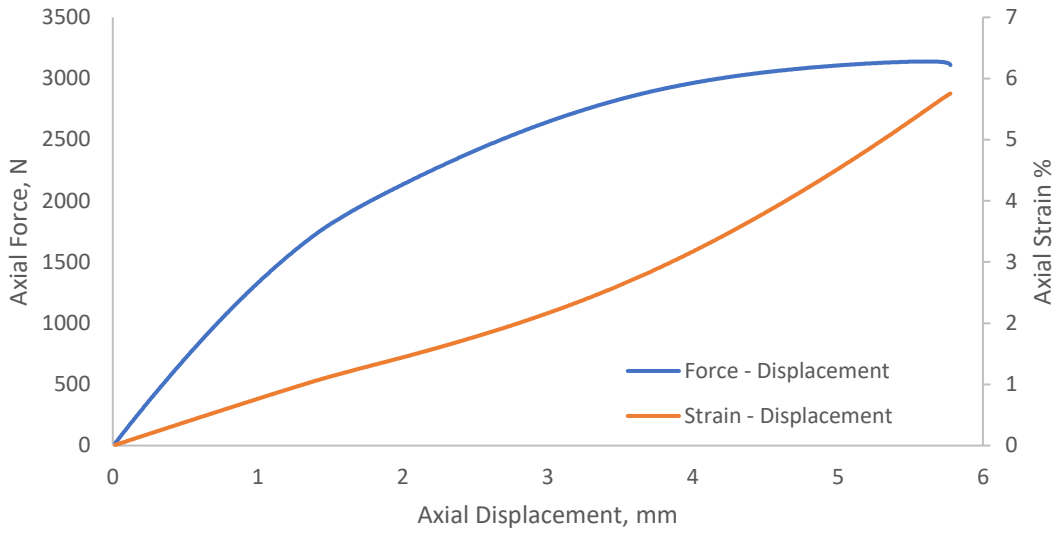

Figure 29: Force & Strain vs. Displacement for B-0

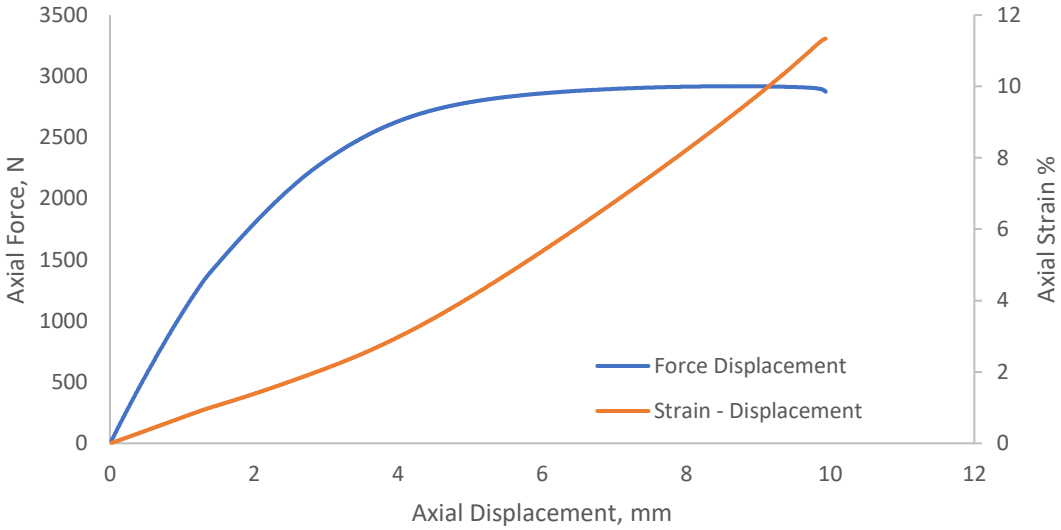

Figure 30: Force & Strain vs. Displacement for B-45

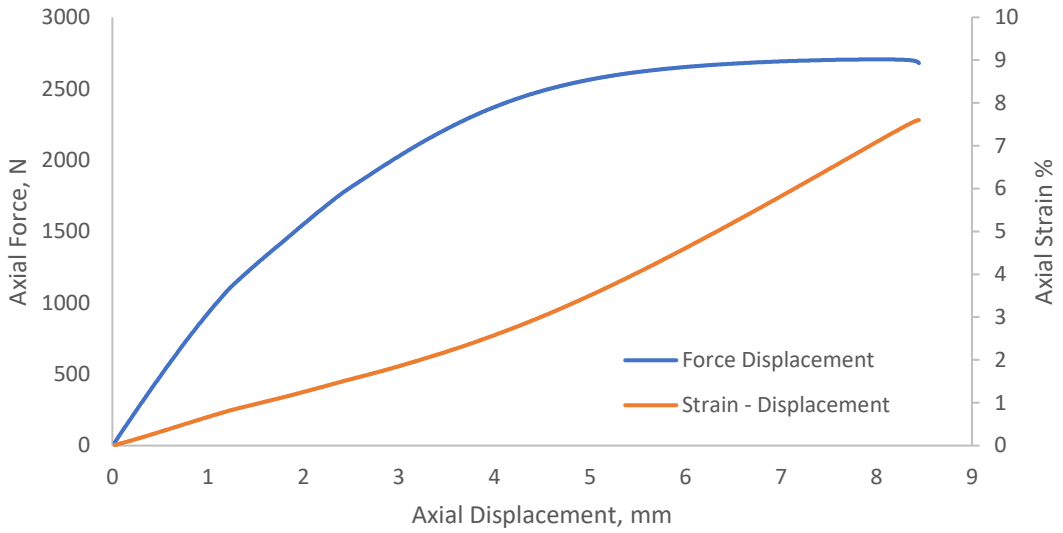

Figure 31: Force & Strain vs. Displacement for B-90

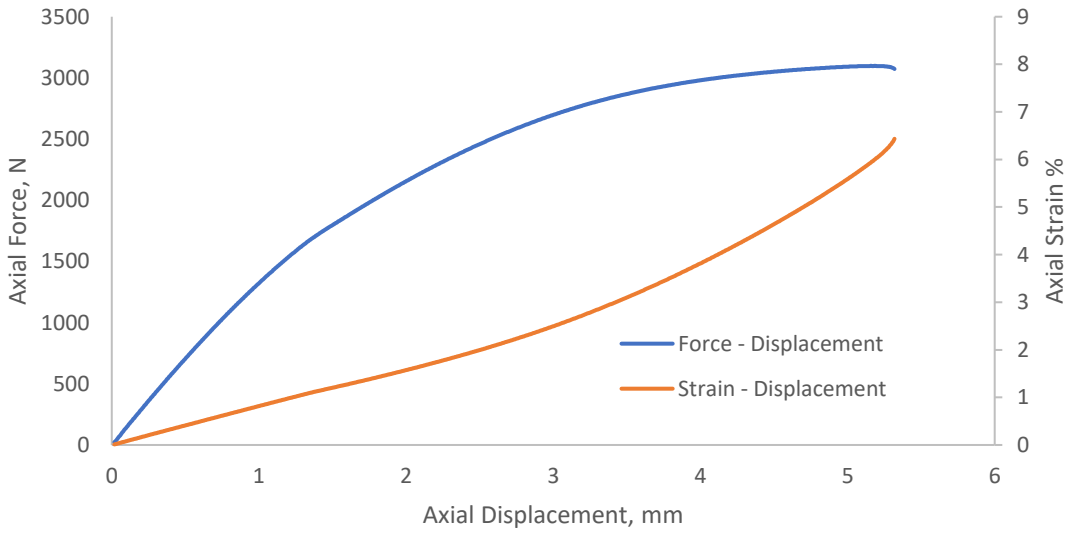

Figure 32: Force & Strain vs. Displacement for C-0

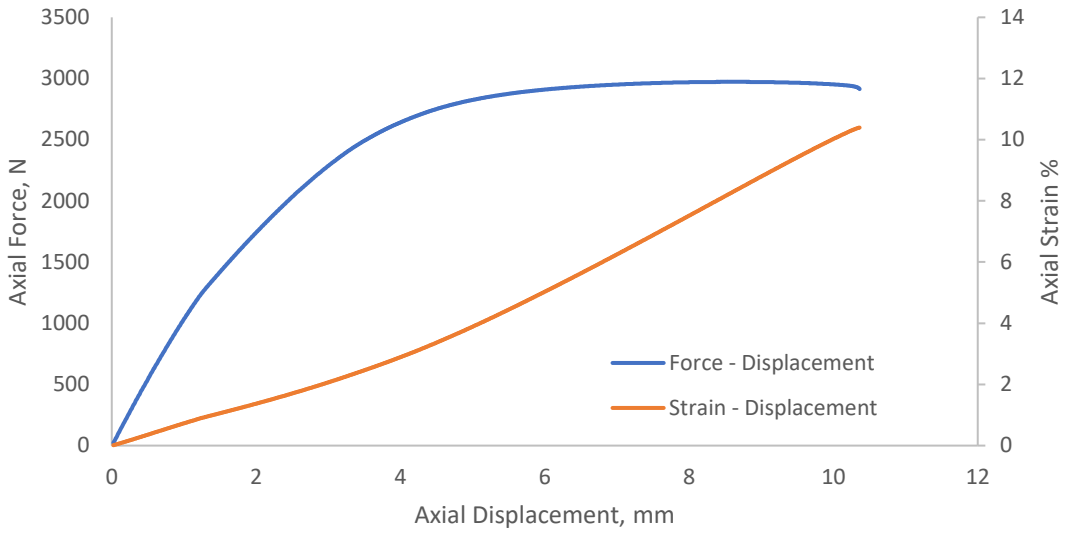

Figure 33: Force & Strain vs. Displacement for C-45

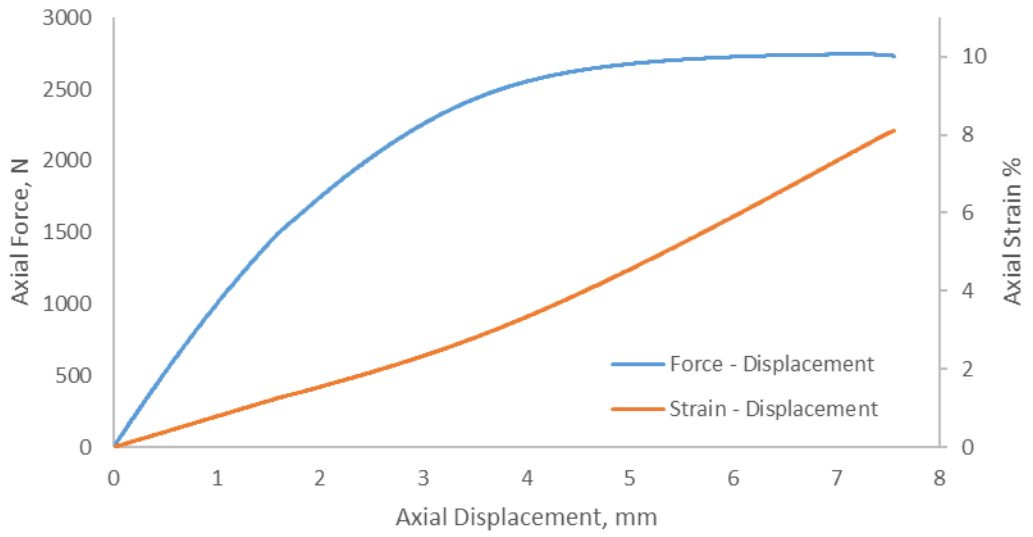

Figure 34: Force & Strain vs. Displacement for C-90

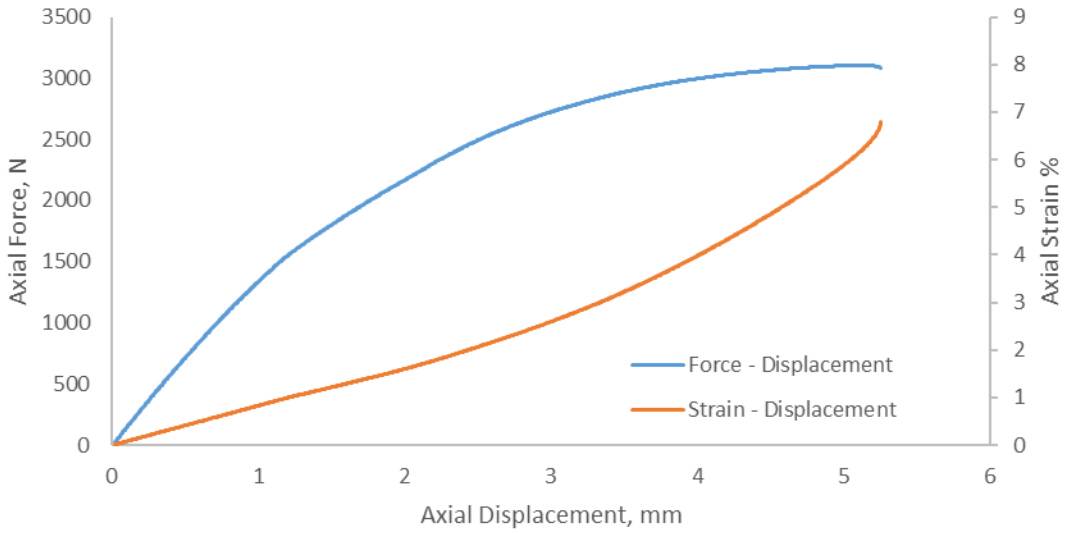

Figure 35: Force & Strain vs. Displacement for D-0

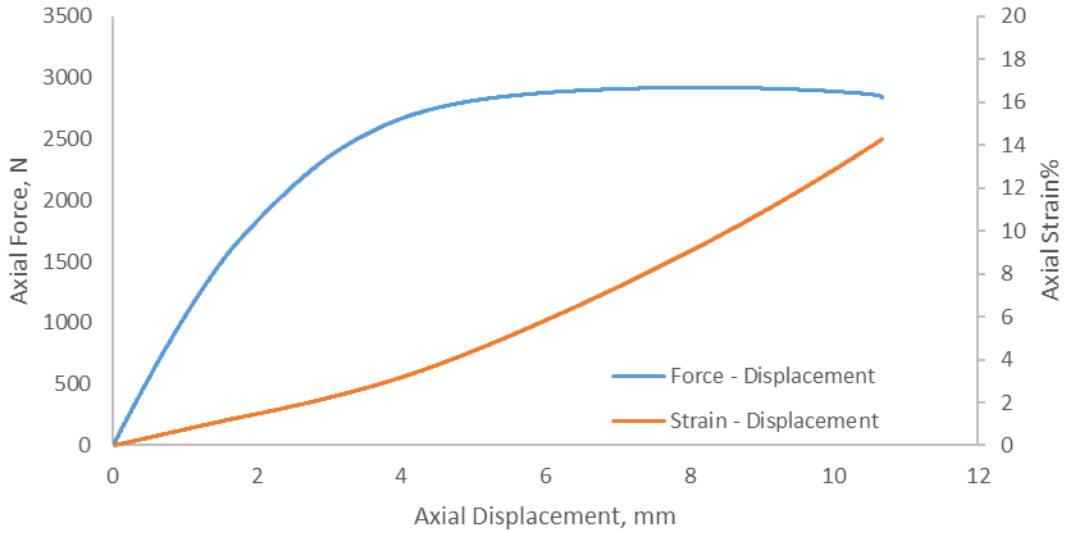

Figure 36: Force & Strain vs. Displacement for D-45

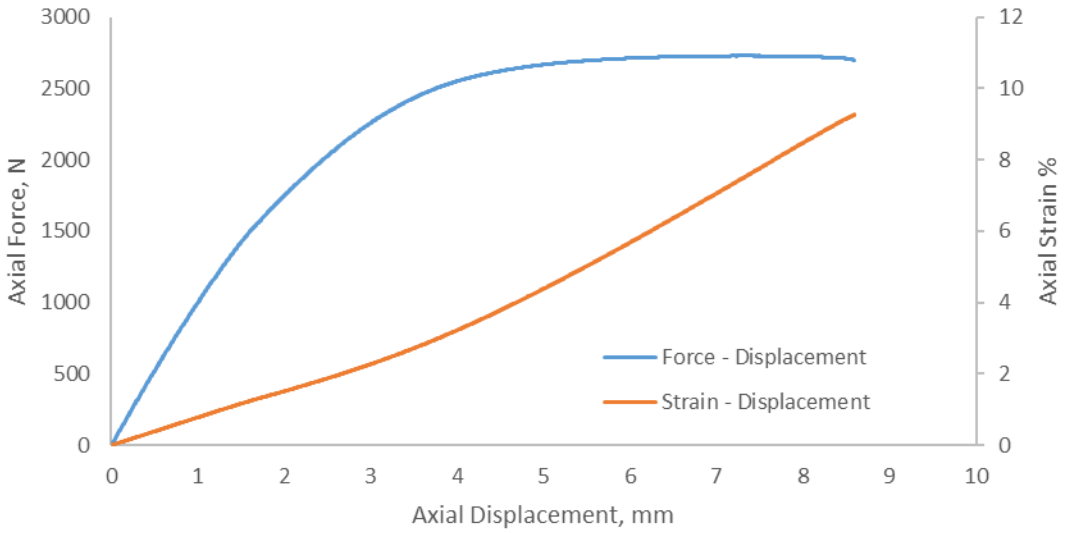

Figure 37: Force & Strain vs. Displacement for D-90

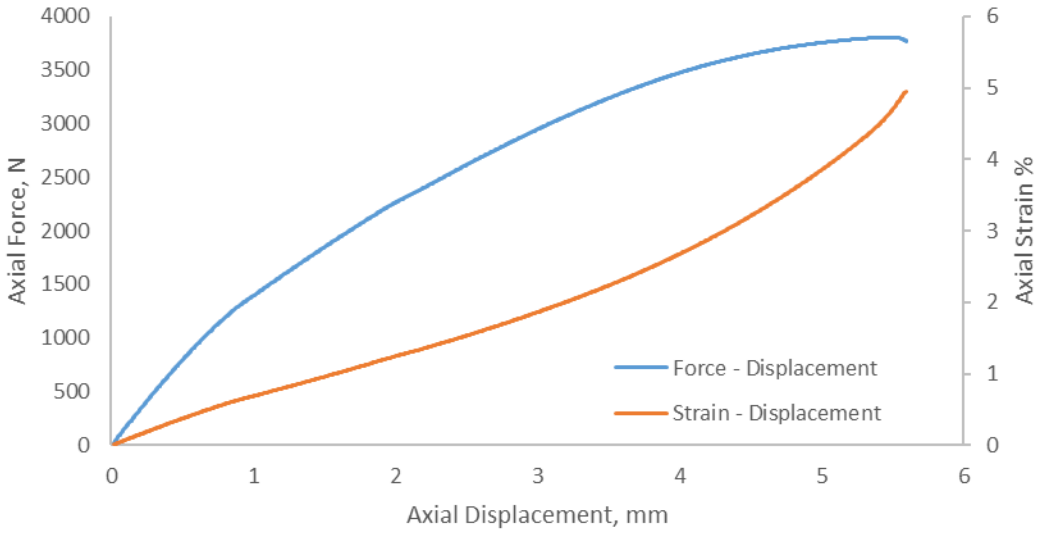

Figure 38: Force & Strain vs. Displacement for E-0

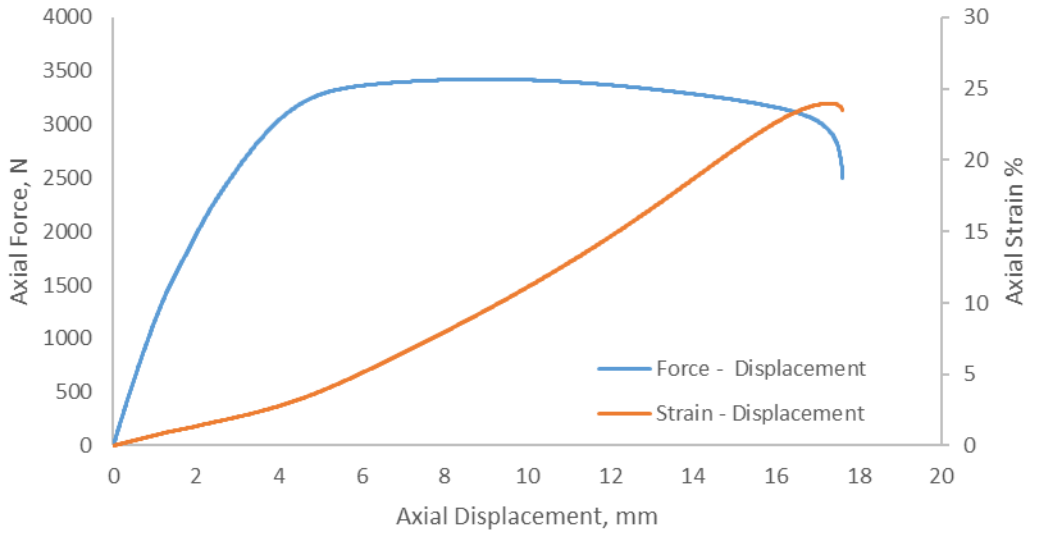

Figure 39: Force & Strain vs. Displacement for E-45

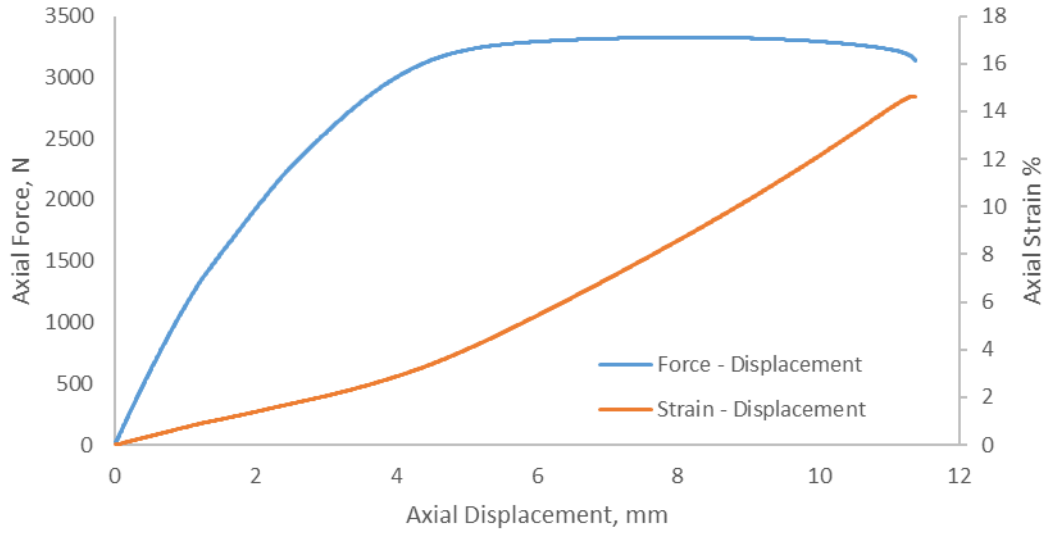

Figure 40: Force & Strain vs. Displacement for E-90

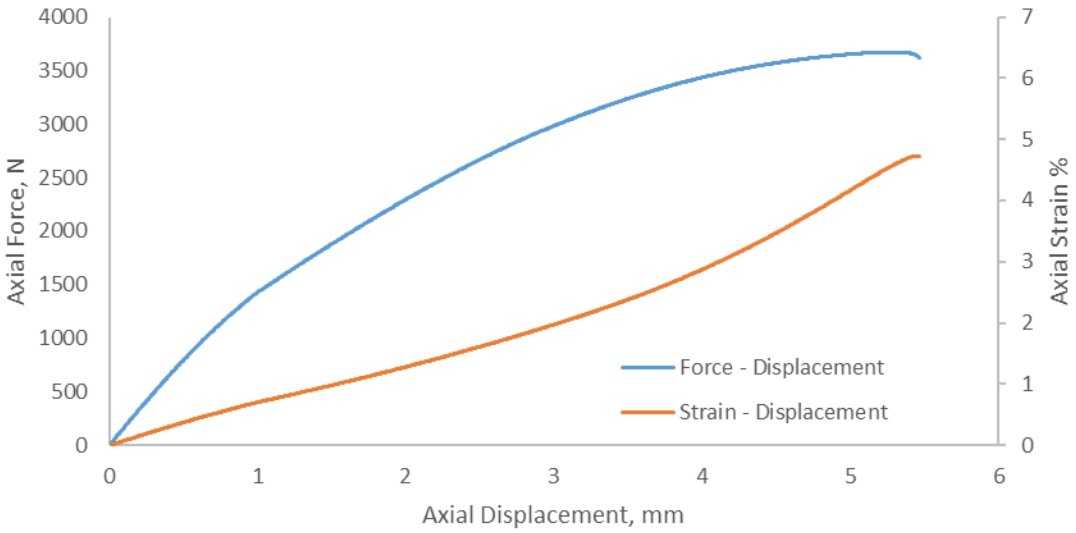

Figure 41: Force & Strain vs. Displacement for F-0

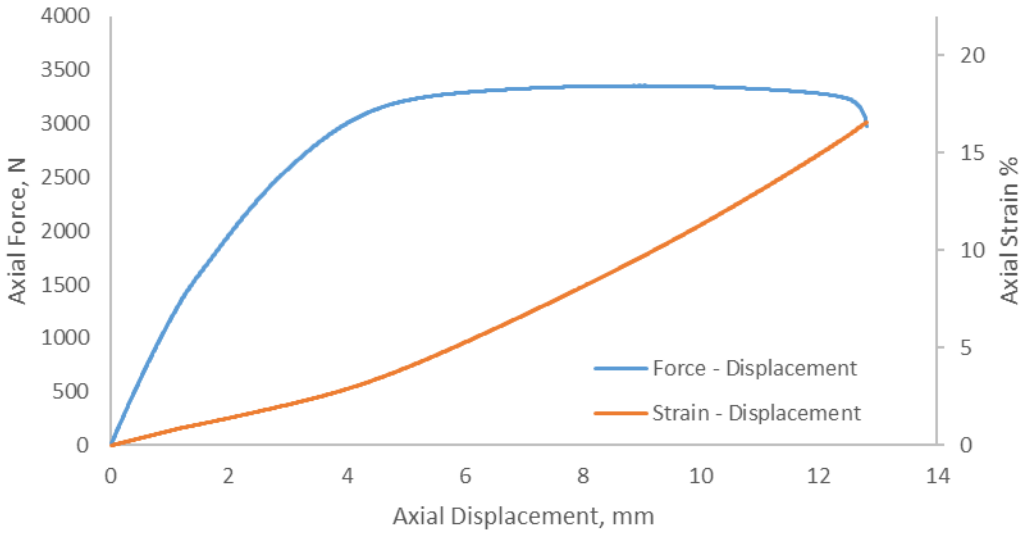

Figure 42: Force & Strain vs. Displacement for F-45

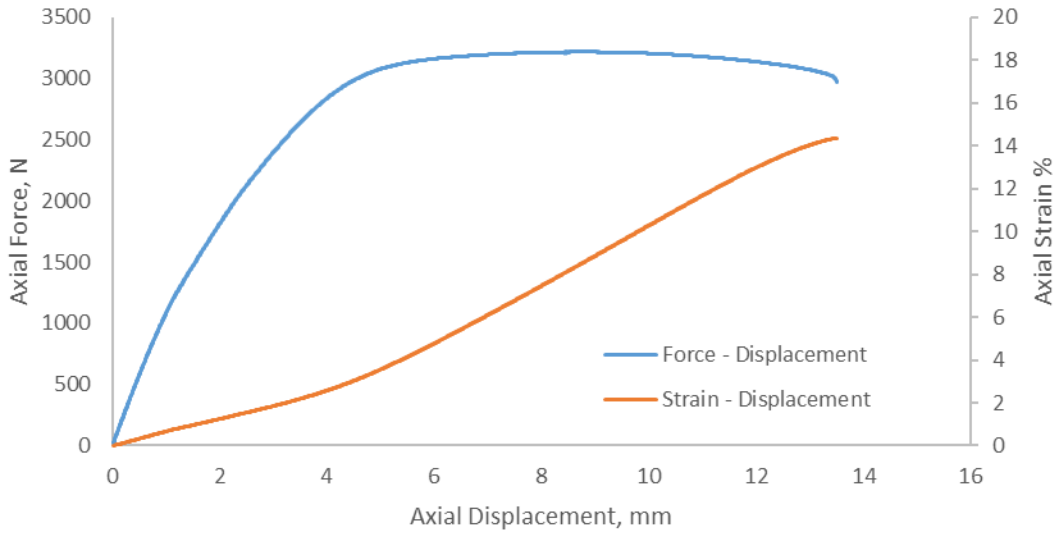

Figure 43: Force & Strain vs. Displacement for F-90

Appendix 3: Stress-Strain Curves

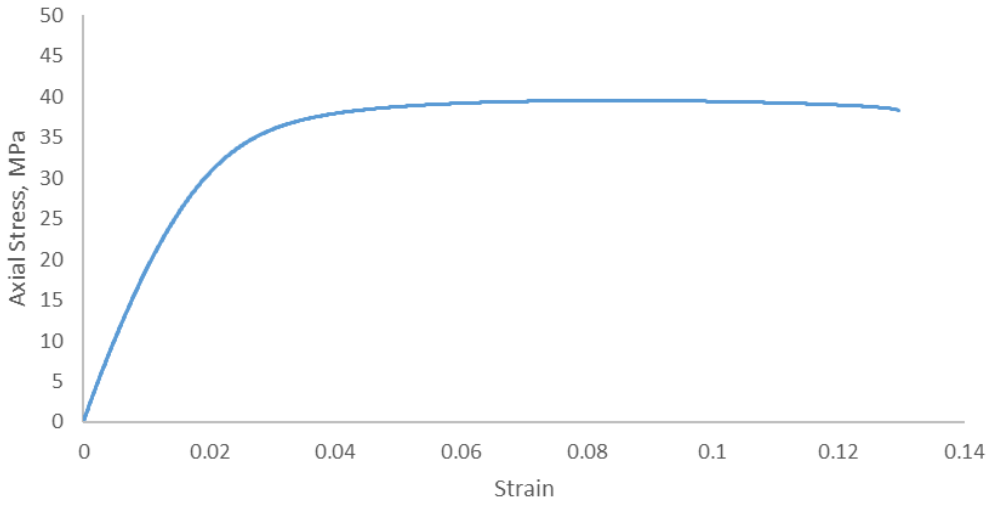

Figure 44: Stress vs. Strain for A-45

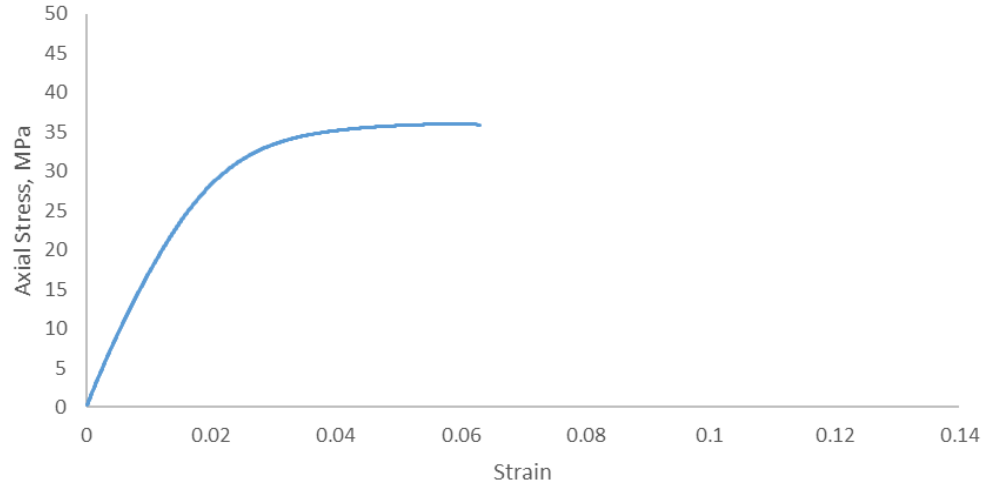

Figure 45: Stress vs. Strain for A-90

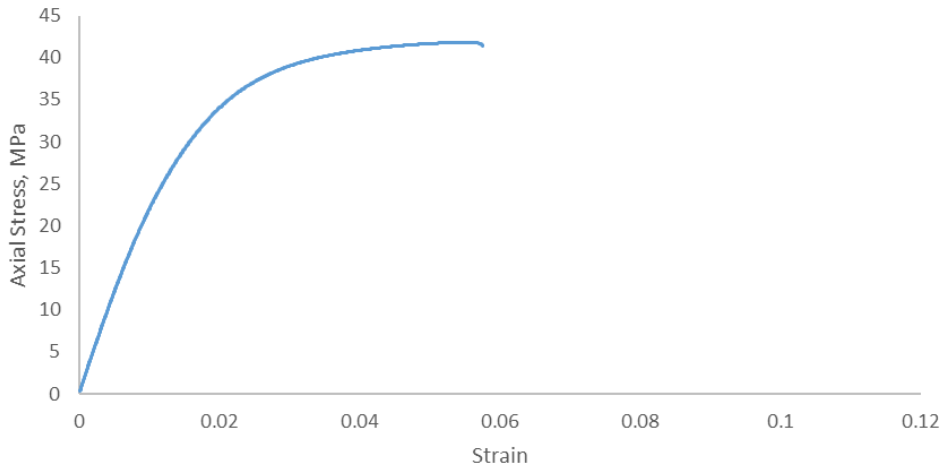

Figure 46: Stress vs. Strain for B-0

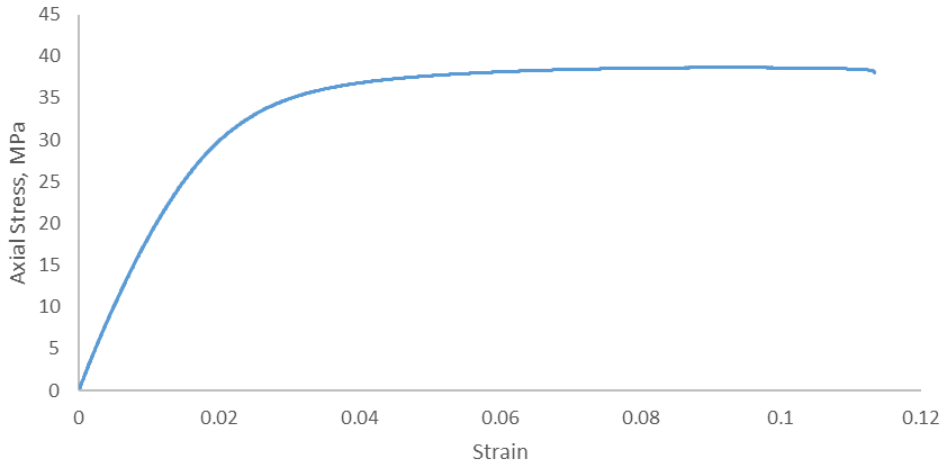

Figure 47: Stress vs. Strain for B-45

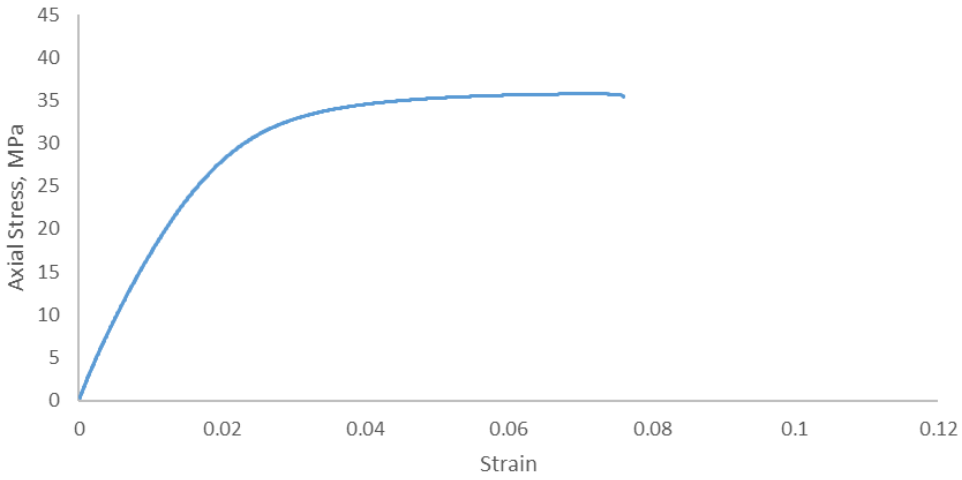

Figure 48: Stress vs. Strain for B-90

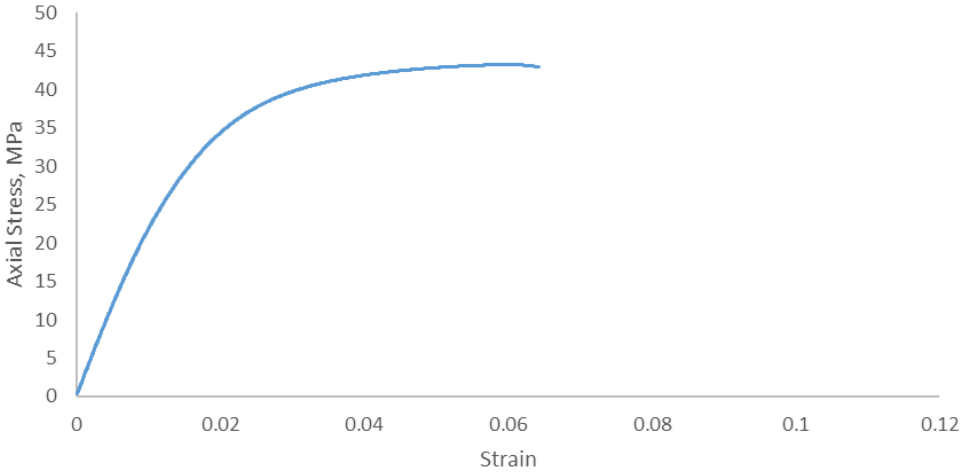

Figure 49: Stress vs. Strain for C-0

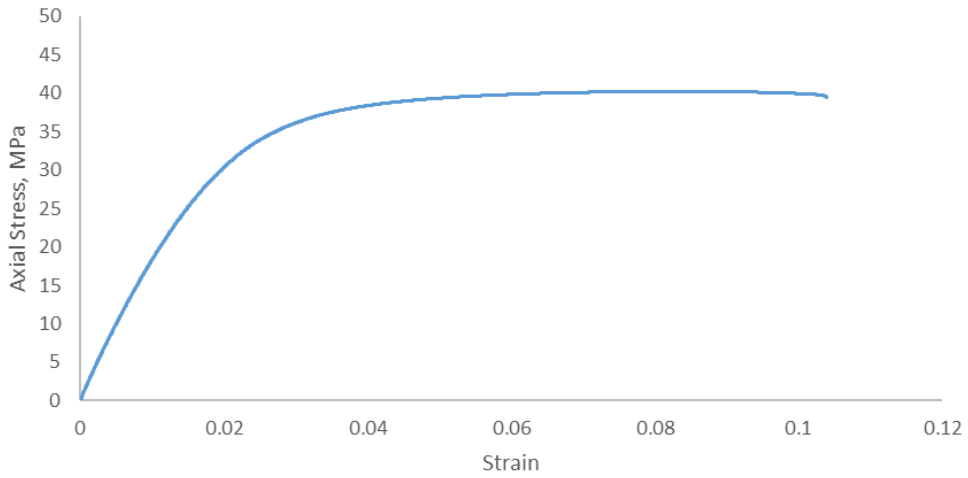

Figure 50: Stress vs. Strain for C-45

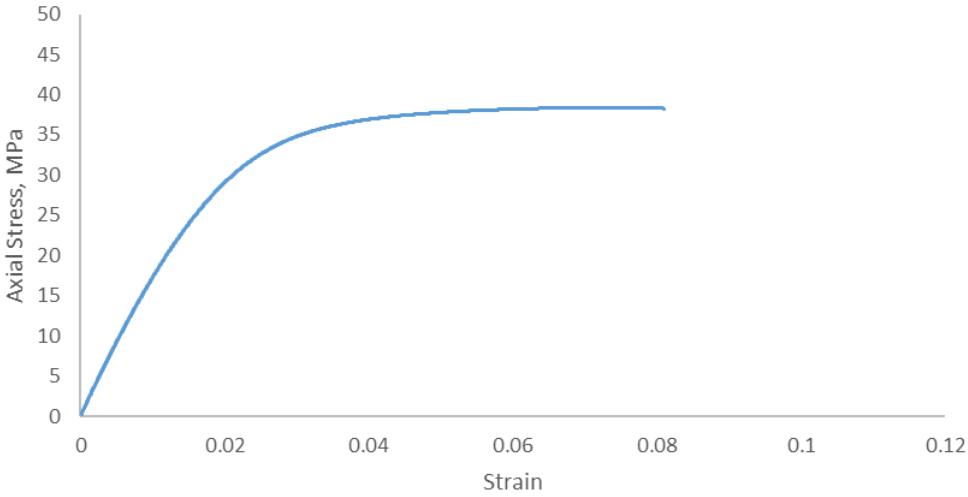

Figure 51: Stress vs. Strain for C-90

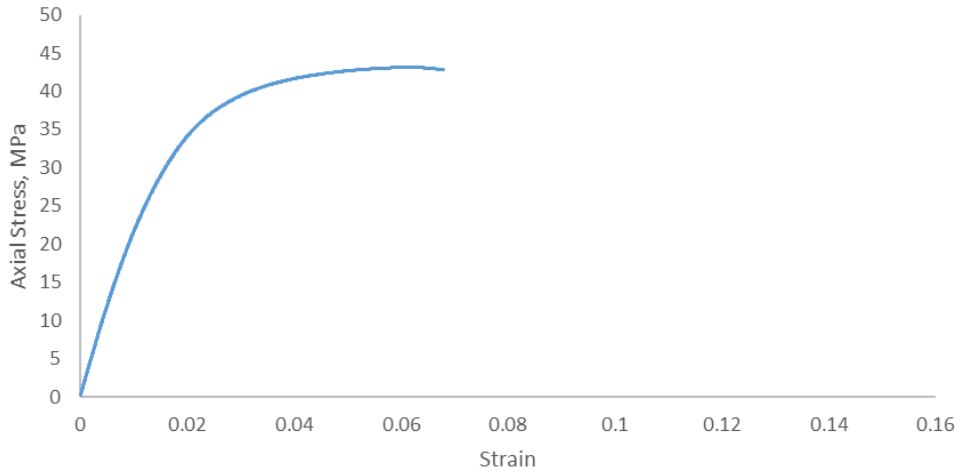

Figure 52: Stress vs. Strain for D-0

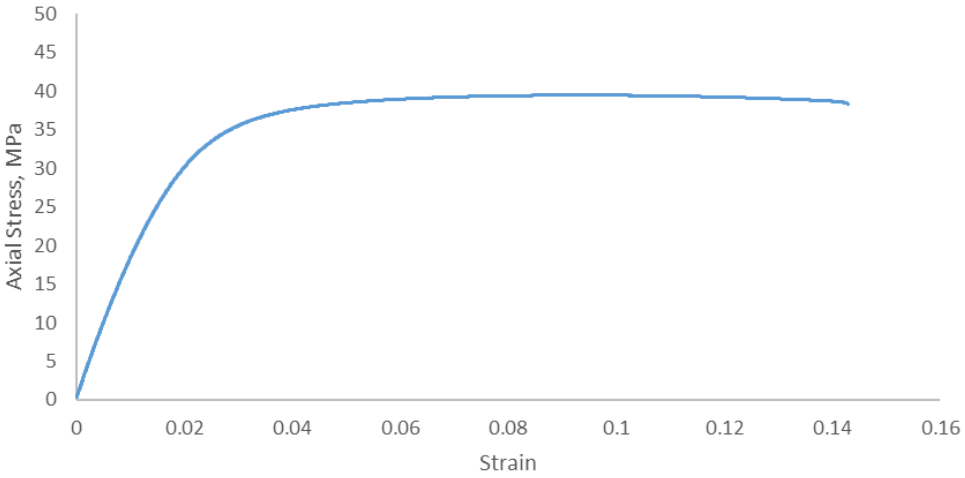

Figure 53: Stress vs. Strain for D-45

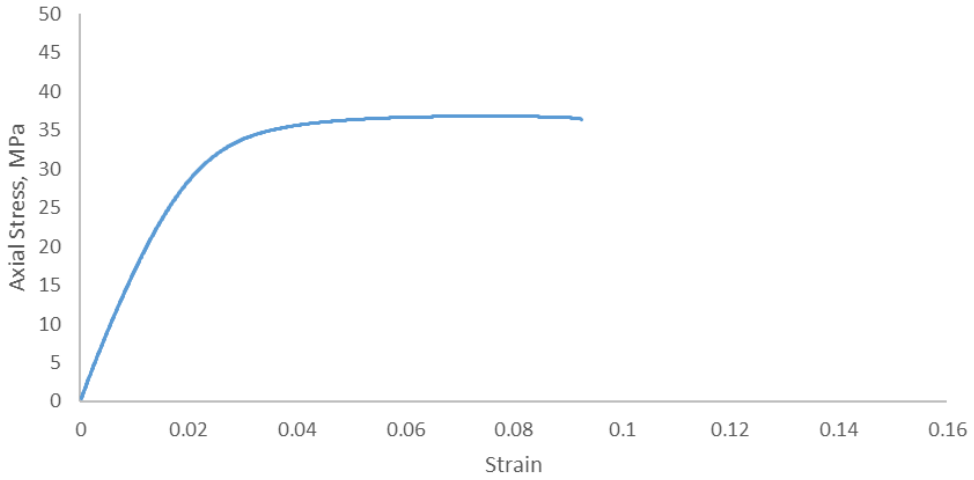

Figure 54: Stress vs. Strain for D-90

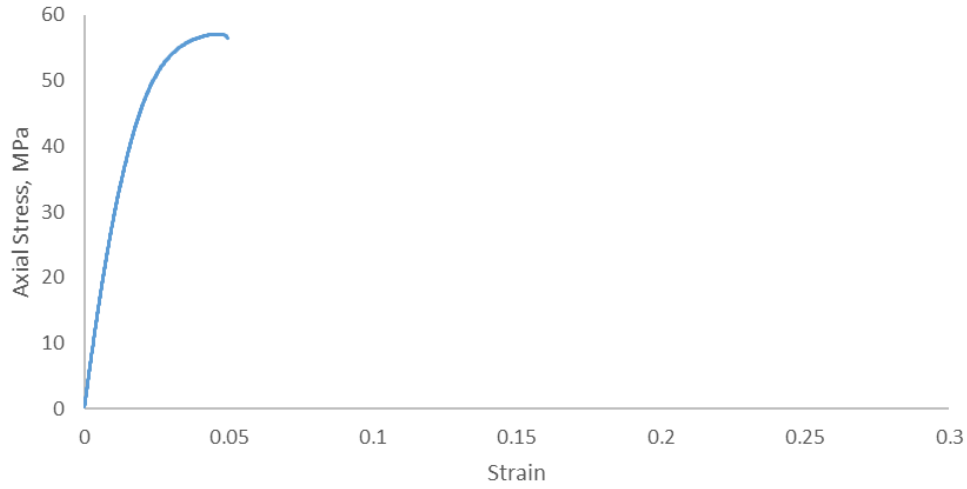

Figure 55: Stress vs. Strain for E-0

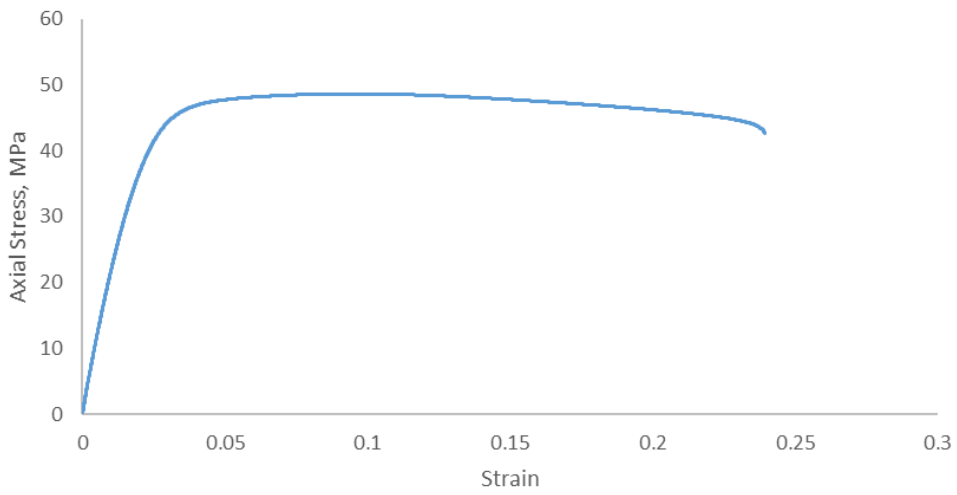

Figure 56: Stress vs. Strain for E-45

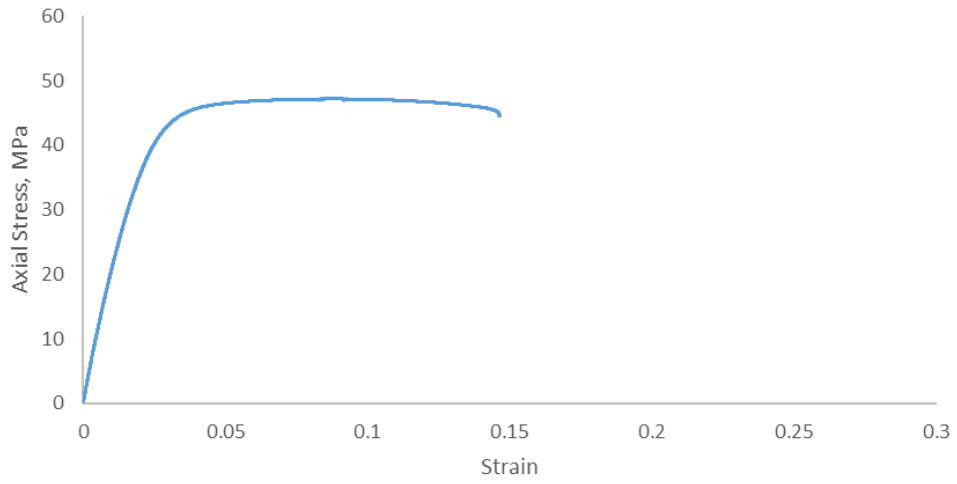

Figure 57: Stress vs. Strain for E-90

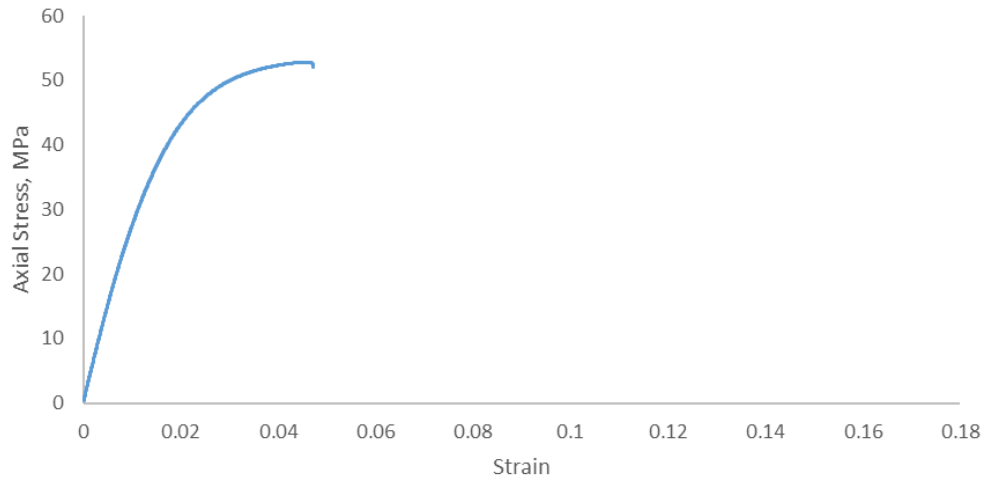

Figure 58: Stress vs. Strain for F-0

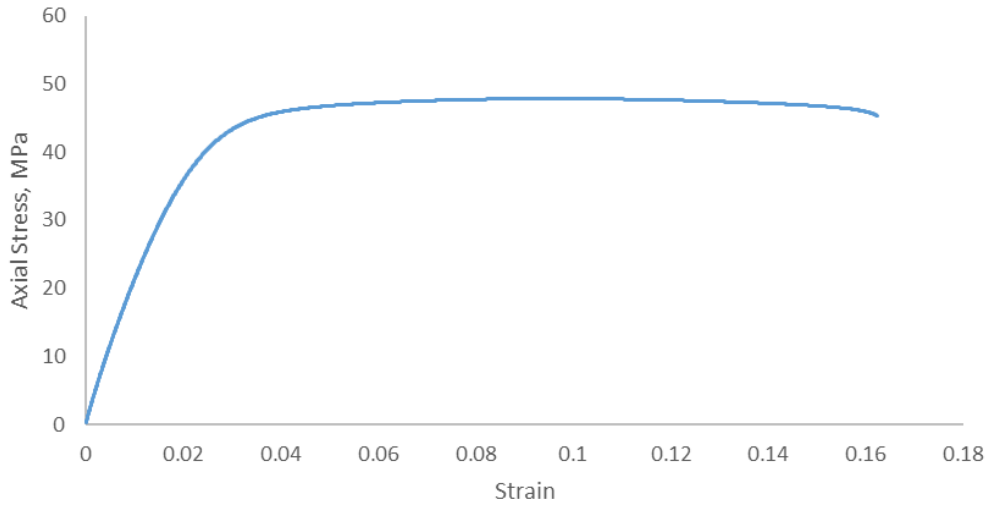

Figure 59: Stress vs. Strain for F-45

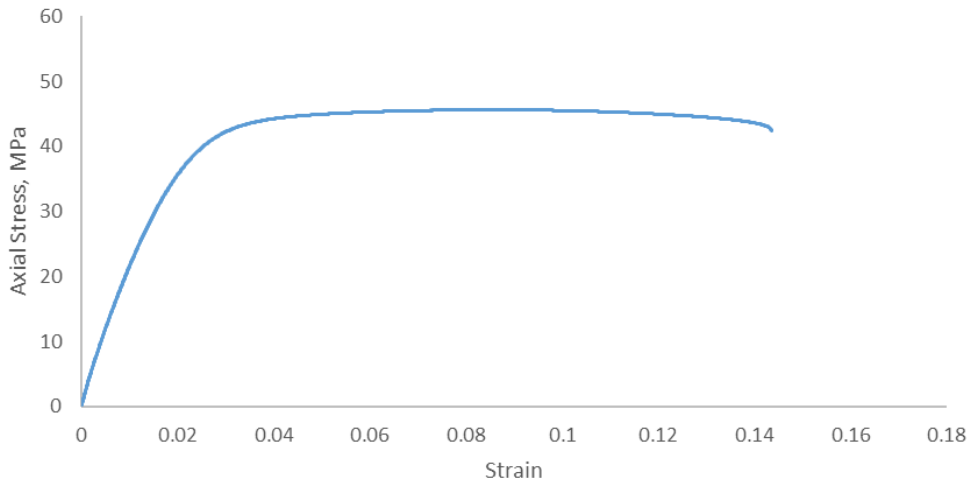

Figure 60: Stress vs. Strain for F-90

Appendix 4: Estimates of Young's Modulus

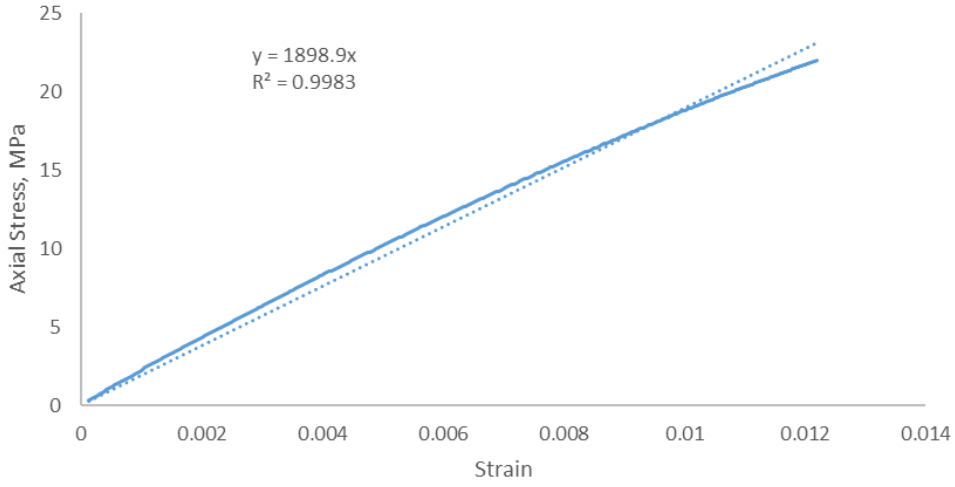

Figure 61: Initial portion of the stress vs. strain plot for A-45

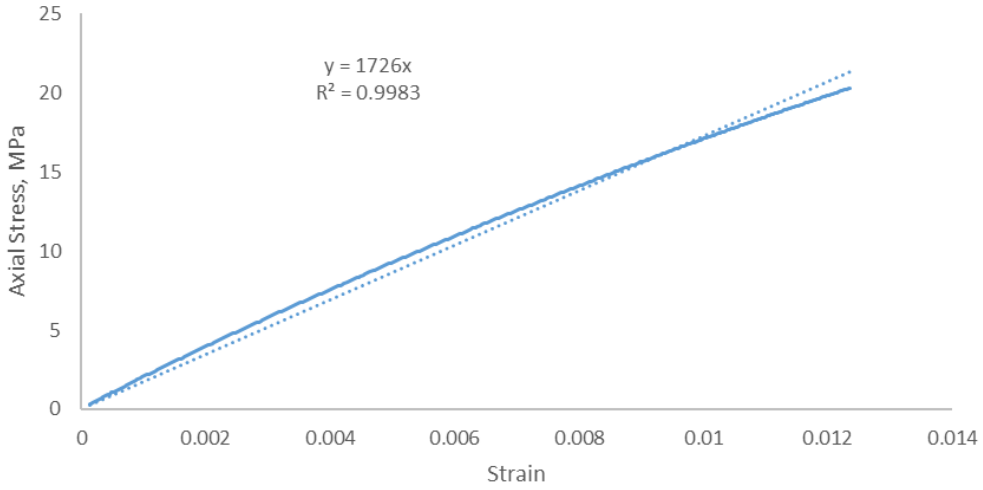

Figure 62: Initial portion of the stress vs. strain plot for A-90

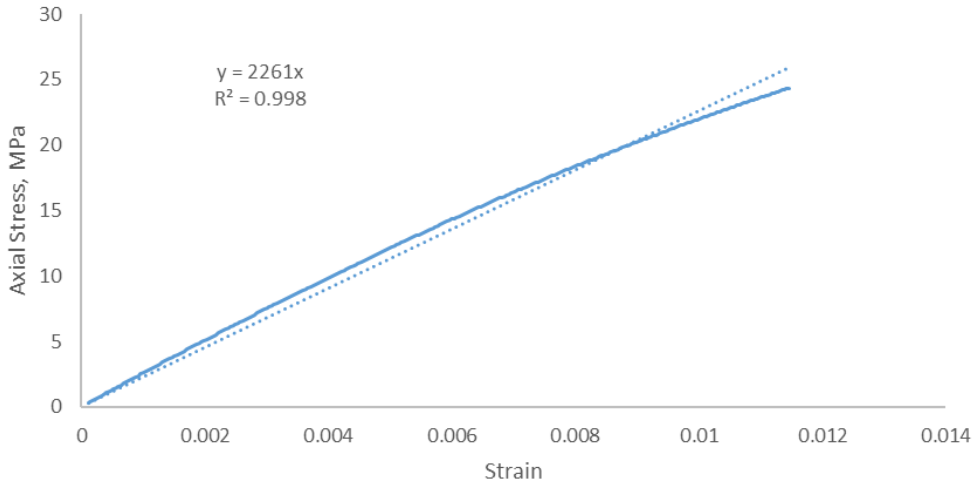

Figure 63: Initial portion of the stress vs. strain plot for B-0

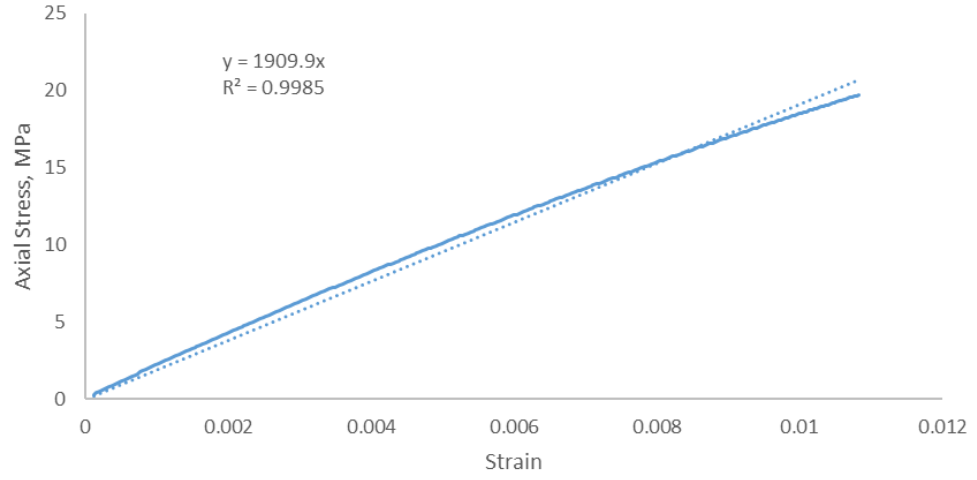

Figure 64: Initial portion of the stress vs. strain plot for B-45

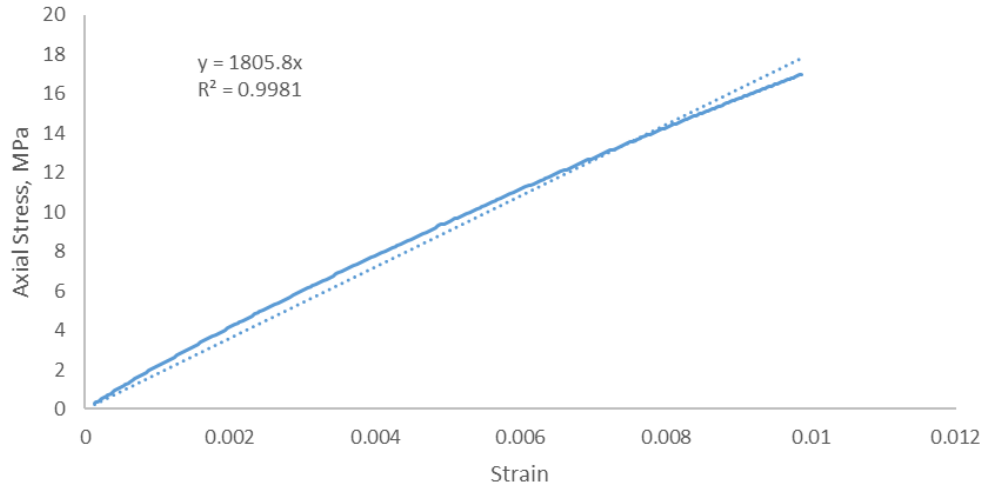

Figure 65: Initial portion of the stress vs. strain plot for B-90

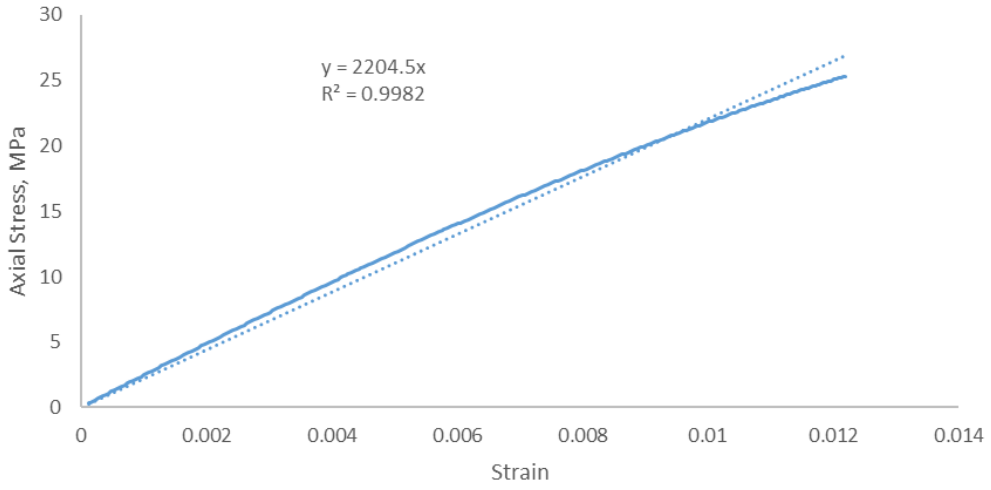

Figure 66: Initial portion of the stress vs. strain plot for C-0

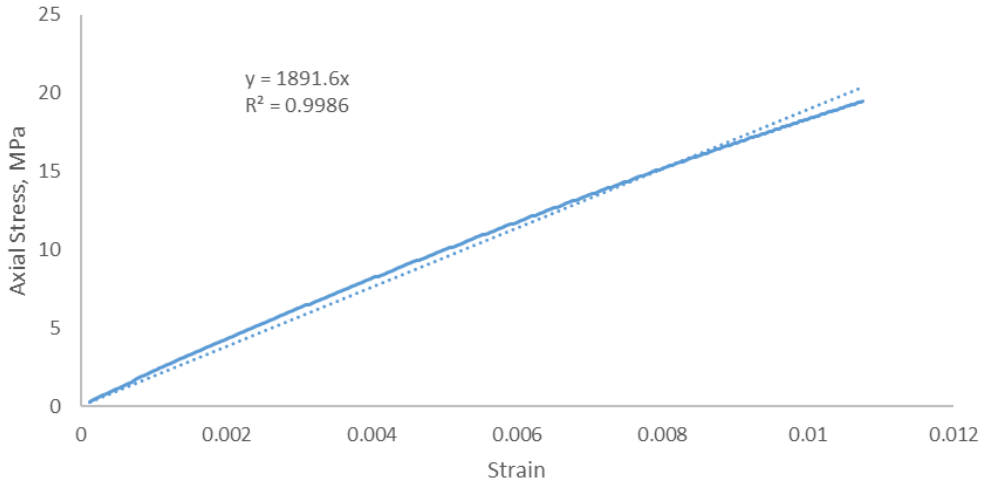

Figure 67: Initial portion of the stress vs. strain plot for C-45

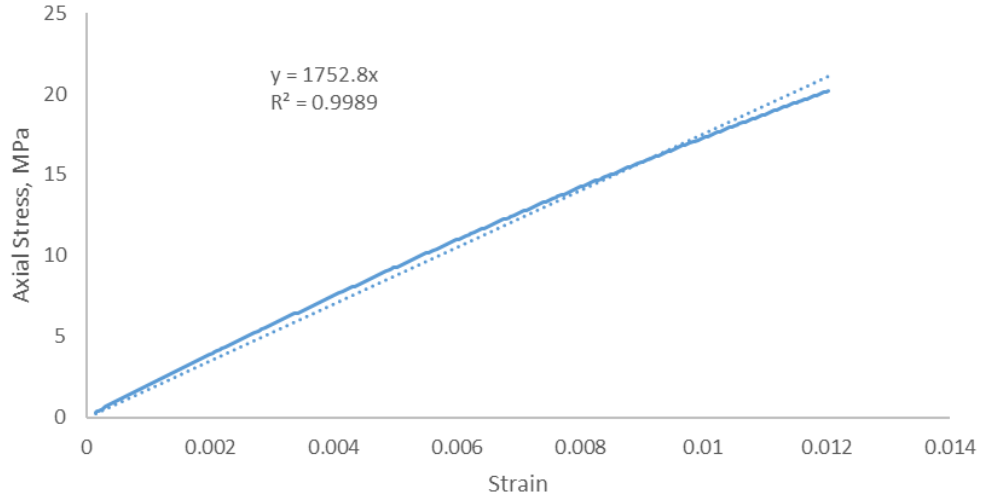

Figure 68: Initial portion of the stress vs. strain plot for C-90

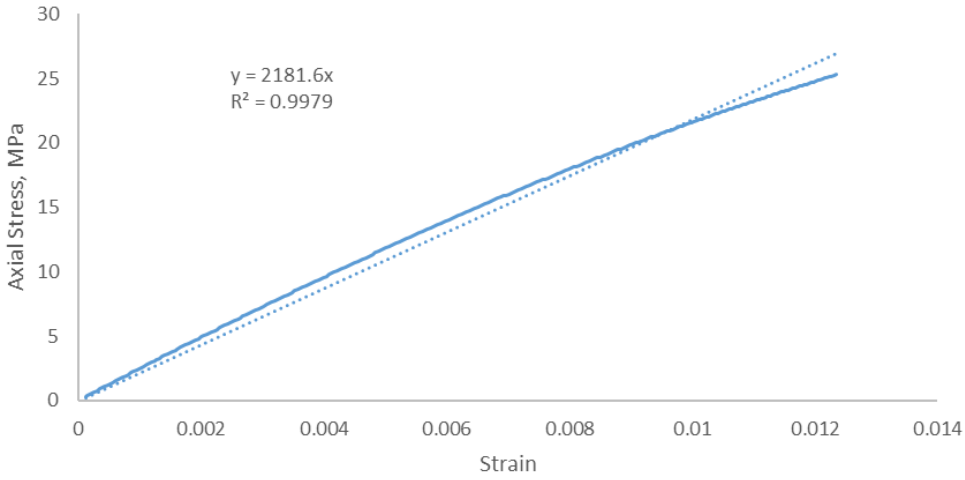

Figure 69: Initial portion of the stress vs. strain plot for D-0

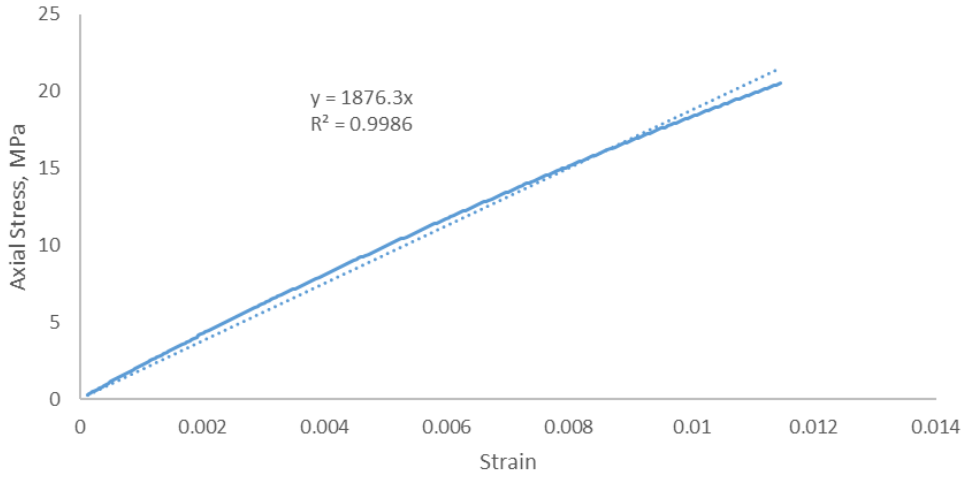

Figure 70: Initial portion of the stress vs. strain plot for D-45

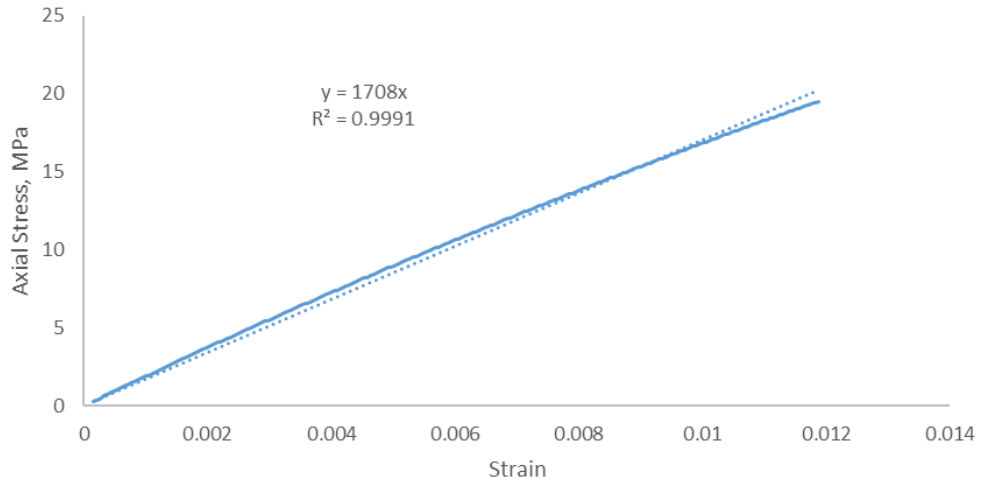

Figure 71: Initial portion of the stress vs. strain plot for D-90

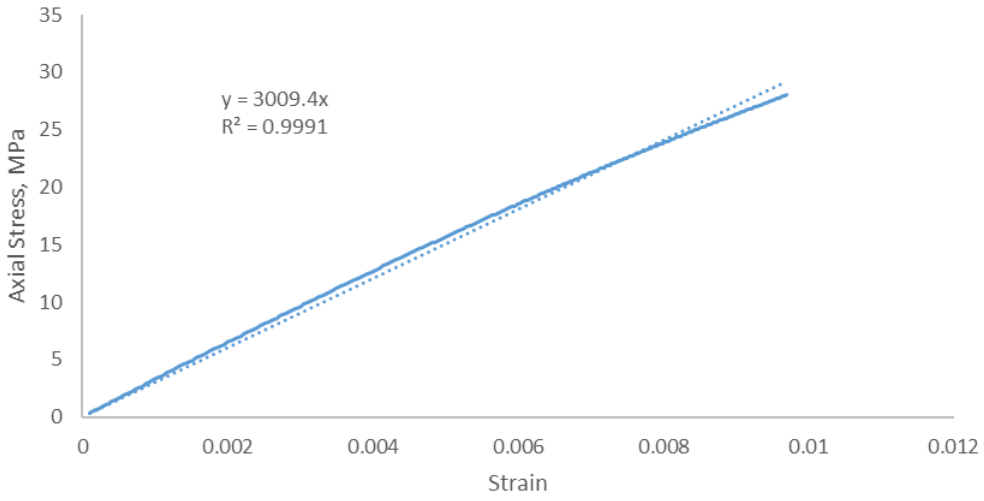

Figure 72: Initial portion of the stress vs. strain plot for E-0

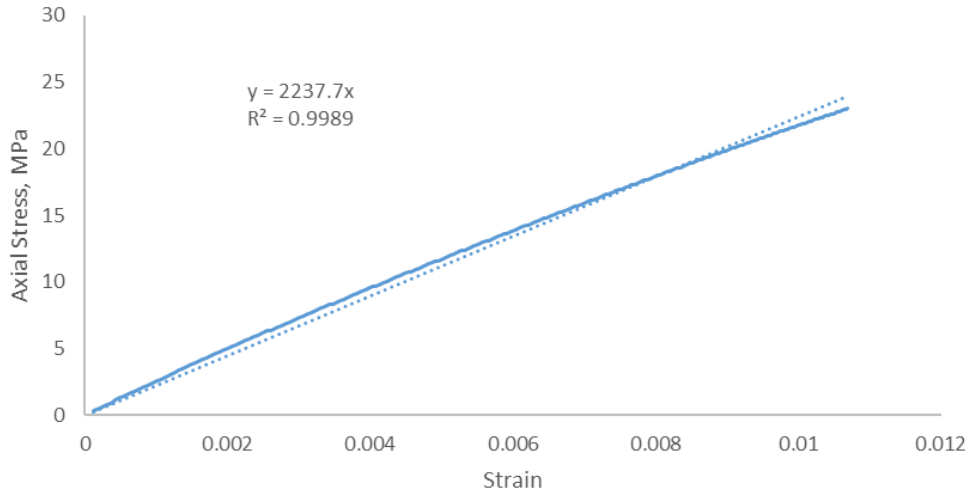

Figure 73: Initial portion of the stress vs. strain plot for E-45

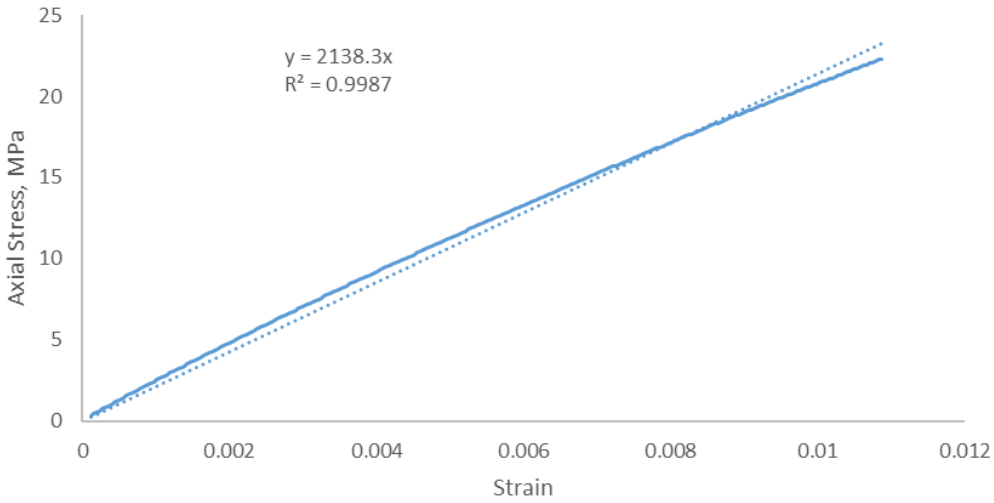

Figure 74: Initial portion of the stress vs. strain plot for E-90

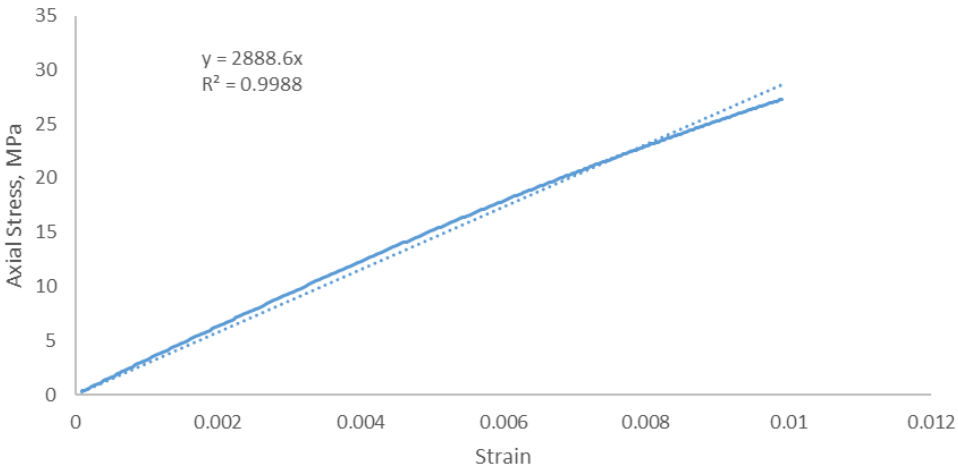

Figure 75: Initial portion of the stress vs. strain plot for F-0

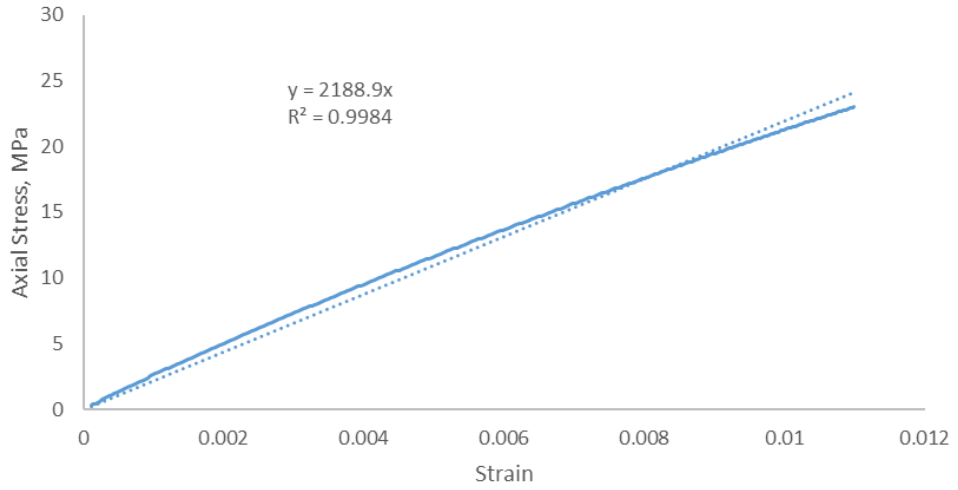

Figure 76: Initial portion of the stress vs. strain plot for F-45

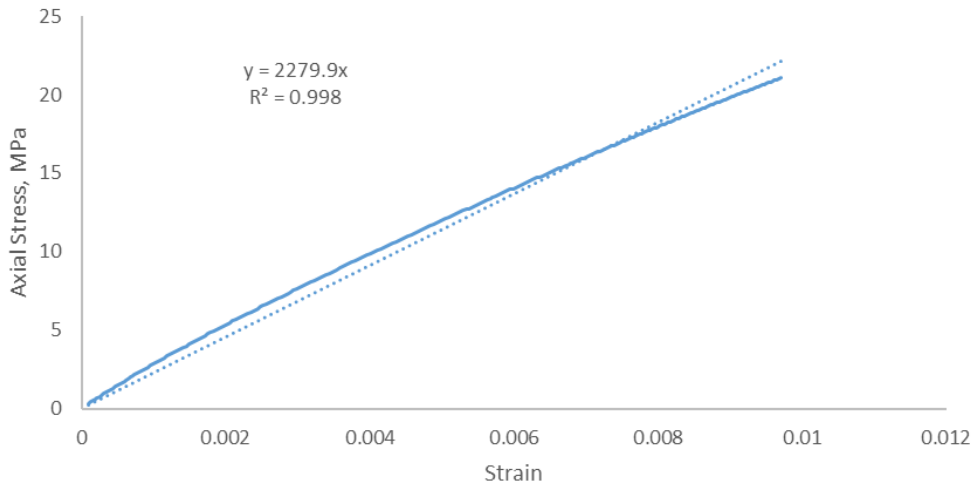

Figure 77: Initial portion of the stress vs. strain plot for F-90